# Crustal structure of the northern Main Ethiopian Rift from the EAGLE controlled-source survey; a snapshot of incipient lithospheric break-up

P.K.H. MAGUIRE[1], G.R. KELLER[2], S.L. KLEMPERER[3], G.D. MACKENZIE[1,*], K. KERANEN[3], S. HARDER[2], B. O'REILLY[4], H. THYBO[5], L. ASFAW[6], M.A. KHAN[1] AND M. AMHA[7]

[1]*Department of Geology, University of Leicester, Leicester LE1 7RH, UK (e-mail: pkm@le.ac.uk)*

[2]*Department of Geological Sciences, University of Texas at El Paso, El Paso, TX 79968, USA*

[3]*Department of Geophysics, Stanford University, Stanford, CA94305-2215, USA*

[4]*Dublin Institute of Advanced Studies, 5 Merrion Square, Dublin, Ireland*

[5]*Geological Institute, University of Copenhagen, Oster Voldgade 10, DK-1350, Copenhagen, Denmark*

[6]*Geophysical Observatory, Addis Ababa University, P.O. Box 1176, Addis Ababa, Ethiopia*

[7]*Ethiopian Science and Technology Commission, P.O. Box 2490, Addis Ababa, Ethiopia*

[*]*Now at: Compagnie Générale de Géophysique, Vantage West, Great West Rd., Brentford, Middlesex, TW8 9GG, UK*

**Abstract:** The Ethiopia Afar Geoscientific Lithospheric Experiment (EAGLE) was undertaken to provide a snapshot of lithospheric break-up above a mantle upwelling at the transition between continental and oceanic rifting. The focus of the project was the northern Main Ethiopian Rift (NMER) cutting across the uplifted Ethiopian plateau comprising the Eocene–Oligocene Afar flood basalt province. A major component of EAGLE was a controlled-source seismic survey involving one rift-axial and one cross-rift *c*. 400 km profile, and a *c*. 100 km diameter 2D array to provide a 3D subsurface image beneath the profiles' intersection. The resulting seismic data are interpreted in terms of a crustal and sub-Moho P-wave seismic velocity model. We identify four main results: (1) the velocity within the mid- and upper crust varies from 6.1 km $s^{-1}$ beneath the rift flanks to 6.6 km $s^{-1}$ beneath overlying Quaternary axial magmatic segments, interpreted in terms of the presence of cooled gabbroic bodies arranged en echelon along the axis of the rift; (2) the existence of a high-velocity body ($V_p$ 7.4 km $s^{-1}$) in the lower crust beneath the northwestern rift flank, interpreted in terms of about 15 km-thick, mafic underplated/intruded layer at the base of the crust (we suggest this was emplaced during the eruption of Oligocene flood basalts and modified by more recent mafic melt during rifting); (3) the variation in crustal thickness along the NMER axis from *c*. 40 km in the SW to *c*. 26 km in the NE beneath Afar. This variation is interpreted in terms of the transition from near-continental rifting in the south to a crust in the north that could be almost entirely composed of mantle-derived mafic melt; and (4) the presence of a possibly continuous mantle reflector at a depth of about 15–25 km below the base of the crust beneath both linear profiles. We suggest this results from a compositional or structural boundary, its depth apparently correlated with the amount of extension.

The northern Main Ethiopian Rift (NMER) lies between the onshore extensions of the southern Red Sea and the Gulf of Aden rifts and the remainder of the East African rift system to the south (Fig. 1). It transects the Ethiopian plateau, a 1000 km-wide Palaeogene flood basalt province at 2500 m elevation (e.g. Mohr & Zanettin 1988), and is thus a prime locale to develop our understanding of the lithospheric processes resulting from continental break-up above what is widely believed to be a mantle plume (e.g. Montelli *et al.* 2004).

As continental rifting proceeds to sea-floor spreading, asthenospheric processes controlling magma supply should begin to dominate over lithospheric mechanical processes in the architecture of

*From*: YIRGU, G., EBINGER, C.J. & MAGUIRE, P.K.H. (eds) 2006. *The Afar Volcanic Province within the East African Rift System.* Geological Society, London, Special Publications, **259**, 269–291.
0305-8719/06/$15.00 

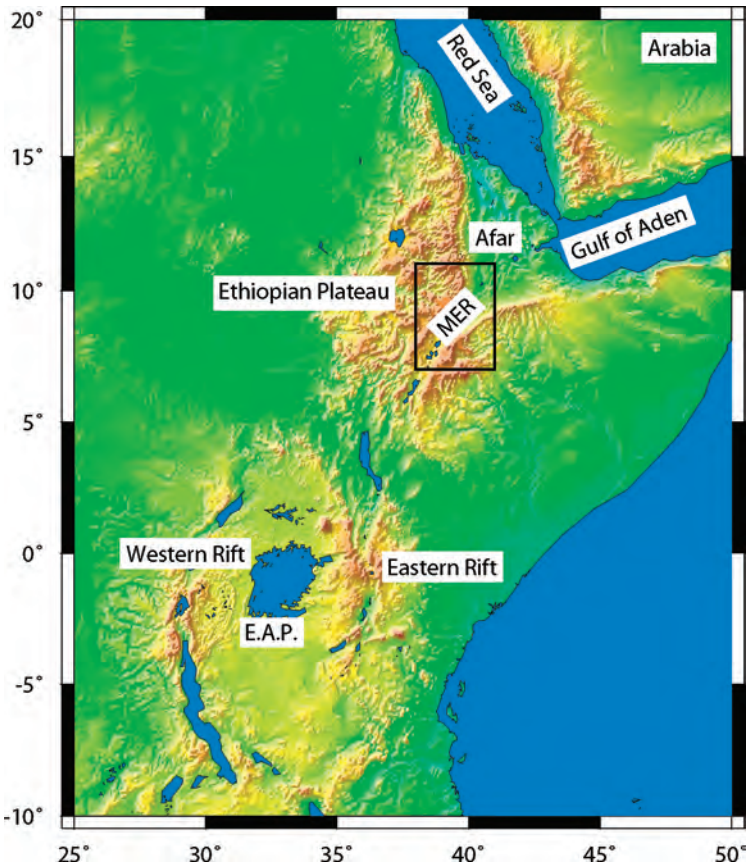


**Fig. 1.** Location map of the East African rift system including the Red Sea, Gulf of Aden, Main Ethiopian Rift (MER), the Eastern (Kenya) rift and the Western rift. Box section indicates region of Fig. 2. Ethiopian plateau is the area of high topography bisected by the MER. E.A.P., East African Plateau.

rifting, extensional strain within the crust being accommodated by axial dyking rather than faulting on rift basin flanking border faults. Ebinger & Casey (2001) proposed such a model for the transitional NMER at the southwestern corner of the Afar depression. Testing this model was a main objective of the Ethiopia Afar Geoscientific Lithospheric Experiment (EAGLE) (Maguire *et al.* 2003).

EAGLE was designed to examine crust and mantle processes occurring beneath the NMER and southern Afar, imaging 3D variations in crustal thickness and upper mantle structure, and characterizing the distribution of strain and magmatism across a typical transitional rift segment. It also involved examination of upper mantle flow associated with rifting above a mantle plume by mapping upper mantle anisotropy (e.g. Kendall *et al.* 2006), thereby providing a snapshot of the lithosphere immediately prior to separation.

A major component of EAGLE was a controlled-source wide-angle reflection/refraction experiment which has resulted in high-resolution 2D seismic velocity models both across and along the axis of the NMER and its transition into Afar, as well as a 3D model of the crustal structure at the intersection of the two 2D profiles. The experiment was designed to complement the EAGLE passive seismic (Bastow *et al.* 2005; Kendall *et al.* 2005, 2006; Stuart *et al.* 2006), local seismicity (Keir *et al.* 2006), magnetotelluric (Whaler & Hautot 2006) and geodetic (Bendick *et al.* 2006) studies. The controlled-source experiment has resulted in a model of absolute crustal and upper-mantle seismic P-wave velocities beneath the NMER providing:

(1) estimates of crustal thinning along and across this transitional sector of the rift, to relate to

present geodetic strain and the geodynamic processes resulting in lithospheric break-up;
(2) a model for the distribution of magmatism within the crust beneath the rift, and its relationship to the surface distribution of magmatic segments and rift architecture;
(3) information on the distribution of magmatic underplate and its contribution to surface uplift, with implications concerning support for the Ethiopian plateau; and
(4) the necessary control on starting models for local earthquake tomography, and the conversion of teleseismic receiver functions to depth.

We report here the first results and implications of this controlled-source seismic programme.

## Tectonic and geological setting

The collision between East and West Gondwana had a profound effect on the geology of East Africa. The late Proterozoic Mozambique belt, representing a Himalayan-scale orogeny, abuts the Archaean complexes of western Ethiopia and the Nyanza craton to the west of the Eastern (Kenya) rift (e.g. Stern 1994). In Ethiopia, the belt is transected by numerous predominantly north–south to NNE–SSW suture zones and associated ophiolitic slivers, and NW–SE trending shear zones (e.g. Abdelsalam & Stern 1996; Allen & Tadesse 2003). Mesozoic marine transgression over this region before the break-up of the Gondwana supercontinent resulted in a thick sedimentary sequence. This was followed in the early Cretaceous by a major tectonic uplift event probably related to rifting in the Sudan (Schull 1988, Bosellini *et al.* 2001). It was followed by deposition of up to 3 km of fluviatile sediments in the area of what is now the Ethiopian plateau and NMER (e.g. Tadesse *et al.* 2003).

The Ethiopian flood-basalt province comprises approximately 350 000 $km^3$ of Oligocene basalts and associated felsic volcanics generated between 31 and 29 Ma following the inferred impact of the Afar mantle plume on the base of the lithosphere. Wolfenden *et al.* (2004) summarize the tectonomagmatic evolution of the region. Extrusion of flood basalts post-dated extension in the Gulf of Aden at *c.* 35 Ma but predated that in the Red Sea at *c.* 28 Ma. Extension began between 18 and 15 Ma in southern Ethiopia, but only after 11 Ma in the NMER where it was associated with further basaltic volcanism (Chernet *et al.* 1998; Bonini *et al.* 2005). Sea-floor spreading in the Gulf of Aden propagated westward into the Afar depression since 16 Ma, and Red Sea sea-floor spreading commenced at *c.* 4 Ma (e.g. d'Acremont *et al.* 2005). Sea-floor spreading has yet to occur in the NMER.

Within the northern Main Ethiopian Rift, structural and stratigraphic patterns indicate a migration of extensional strain from 2.5 Ma to the present, from the marginal border faults to a narrow (20 km) wide-sub-axial zone of narrow, near north–south trending groups of aligned eruptive centres (Wolfenden *et al.* 2004). These in turn are cut by small offset faults and dykes and arranged in a right-stepping en echelon pattern (Boccaletti *et al.* 1999). Recent GPS measurements (Bilham *et al.* 1999) have shown that 80% of the extensional strain is concentrated in these magmatic segments (red-hatched zones in Fig. 2). It is these segments that Ebinger & Casey (2001) proposed as the locus of strain by active dyke injection. Most of the Quaternary volcanism has occurred within these magmatic segments, but other Pliocene–Quaternary volcanic centres are also located near to the NW rift margin (e.g. at Zikwala and Yerer volcanoes (see Fig. 6a)) and on the southeastern rift shoulder (e.g. Chilalo (see Fig. 6a)) demonstrating the spatial complexity of the crust/mantle magmatic system.

Within the rift valley, there are a series of asymmetric structural basins, bounded on one side by steep border faults (*c.* 60 km long and with $>3$ km throw). The basins contain Pleistocene volcanic, clastic and lacustrine strata that overlie the Miocene–Pliocene felsic and mafic sequences of the Kessem and Balchi Formations (Wolfenden *et al.* 2004). These extend into the Debre Zeit area around 8° 45 N. They are assumed to overlie Mesozoic sediments distributed widely over the study area.

## Previous geophysical studies

Recent teleseismic studies have shown that the upper mantle beneath Afar and the northern Main Ethiopian Rift is characterized by an elongate region of low wave-speed anomalies to depths of $>400$ km. The vertical and lateral extent of this anomaly suggests that it originates from a broad thermal upwelling connected to the so-called African superplume in the lower mantle beneath Southern Africa (Benoit *et al.* 2006). Bastow *et al.* (2005) imaged these low velocities as a 75 km-wide sheet extending to depths of around 300 km below the NMER and interpreted the feature as evidence for mantle upwelling. At depths of $>100$ km, north of 8.5° N this low-velocity zone broadens as the rift evolves towards the oceanic spreading centre in Afar, and appears to be connected to the deeper low-velocity structure.

Measurements of seismic anisotropy using regional surface waves demonstrate coherence between sub-lithospheric fast shear-wave orientations and

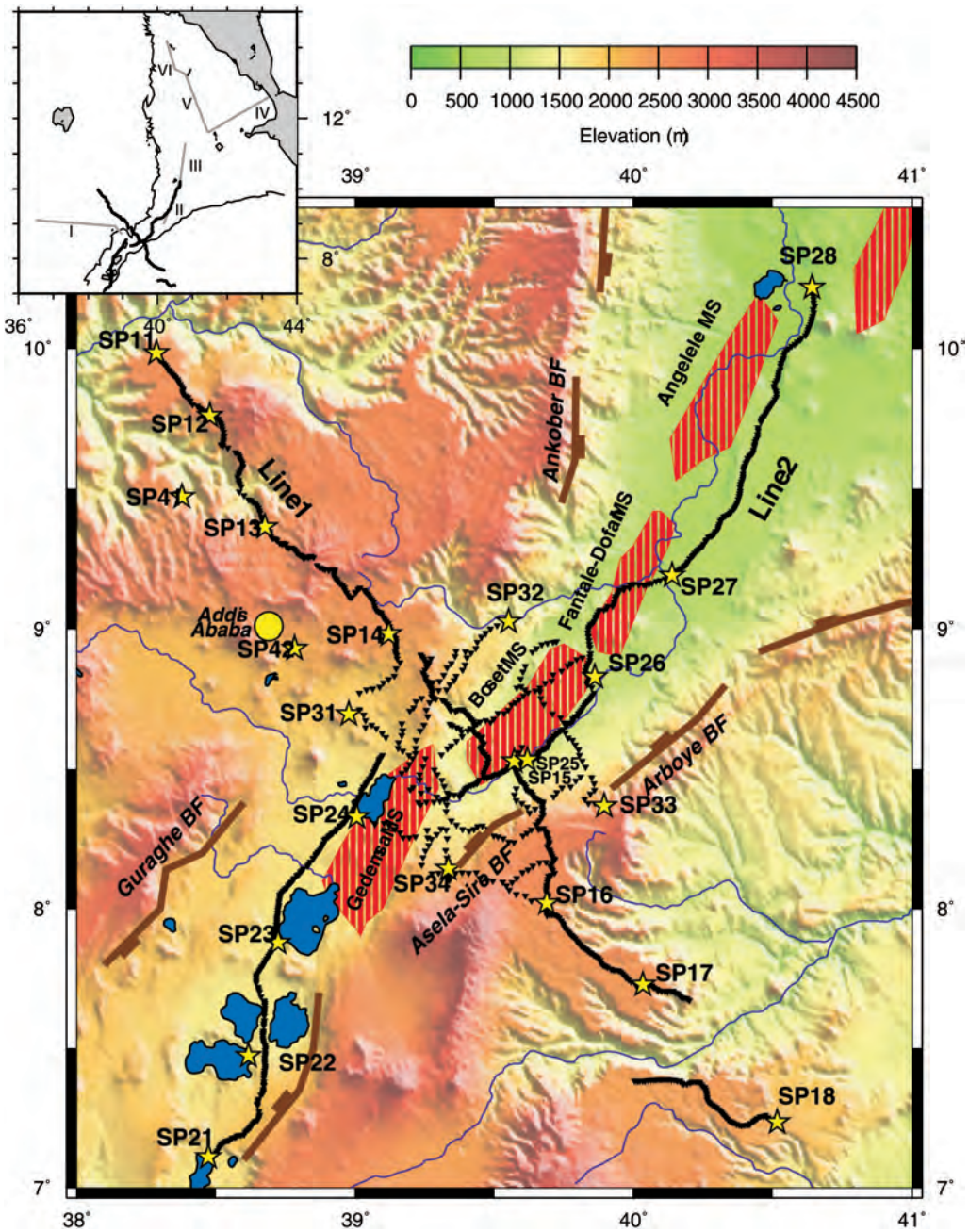


**Fig. 2.** Location map of the EAGLE controlled-source project. Yellow stars, shotpoints (e.g. SP11); black small inverted triangles, controlled source recorders; red hatched areas, magmatic segments (e.g. Boset MS) (after Wolfenden *et al.* 2004); brown lines – border faults (e.g. Arboye BF). Inset map identifies seismic refraction profiles I–VI of Berckhemer *et al.* (1975) in grey, and EAGLE profiles in black.

the trend of the African superplume rising toward the base of the lithosphere beneath Afar (Kendall *et al.* 2006). Above 150 km, the pattern of shear-wave anisotropy is more variable. Analysis of the splitting of teleseismic phase (SKS) and local shear-waves within the rift valley consistently shows rift-parallel directions (Kendall *et al.* 2005; Keir *et al.* 2005). Gashawbeza *et al.* (2004) and Kendall *et al.* (2005) show that the regional lithospheric anisotropy due to Proterozoic accretion of the Mozambique belt is only modified by extensional fabrics within a narrow zone less than 100 km wide beneath the geomorphic rift valley. Average fast shear-wave directions within the rift that are perpendicular to the modern WNW extension direction (Gashawbeza *et al.* 2004) are most likely due to an alignment of $<0.1\%$ melt fraction throughout the upper 70–90 km of the Earth (Kendall *et al.* 2005), parallel to the sheet-like upwelling in the upper mantle. There is a possible increase in the volume of melt from south to north along the rift (Gashawbeza *et al.* 2004). Kendall *et al.* (2006) also show that the anisotropy beneath the Ethiopian plateau is variable and may correspond to both pre-existing fabric and ongoing melt-migration processes.

Despite these significant results, knowledge of crustal structure is needed to evaluate shallow tectonic and magmatic processes in relation to those occurring in the lithospheric mantle and asthenosphere. The only previous crustal refraction data from Ethiopia are six profiles recorded in 1972 with lengths of 120 to 300 km. The recording utilized 15 analogue stations deployed at spacings of 5 to 7 km (Berckhemer *et al.* 1975). They have far lower resolution than our study which utilized over 1000 digital recorders spaced at 1 to 2.5 km. Of the 1972 data, Profile I trending east–west on the western plateau and Profile II coincident with the northern part of our Line 2 are of particular interest; the other profiles are further north in Afar (inset to Fig. 2). Profile I shows an upper crust of velocity 6.1 km s$^{-1}$ and thickness 15 to 23 km above a lower crust of velocity 6.65 km s$^{-1}$. The modelled Moho varied between 33 and 44 km depth (from west to east) above a normal mantle of velocity 8.0 km s$^{-1}$ (Makris & Ginzburg 1987).

Although the 1972 data are too sparse to constrain lateral variations in crustal velocities, Berckhemer *et al.* (1975) note that a high-density lower-crustal body beneath the rift escarpment is required to explain the gravity data. Profile II of Berckhemer *et al.* (1975) shows slightly lower upper-crustal velocities extending to only 8 km depth, above a faster lower crust (6.8 km s$^{-1}$). The highest velocity observed, 7.3 km s$^{-1}$, was presumed to represent partially molten upper mantle beneath the Moho at about 26 km depth. Analysis of the remaining profiles within the Afar region shows crustal thicknesses as low as 16 km (Berckhemer *et al.* 1975). Makris & Ginzburg (1987) provide a modest reinterpretation of the 1972 dataset, including recognition of an upper mantle reflector at *c.* 45 km depth (precise depth dependent on assumed upper-mantle velocity) in southern Afar extending 50 to 100 km north of our northernmost shotpoint SP28. All these older results—within the uncertainties inevitable with their limited recording equipment—are consistent with our newer data discussed below, though some of our geological interpretations differ. For example, Makris & Ginzburg (1987) considered the Afar crust to be continental (albeit stretched and intruded to varying degrees) based on the presence of at least some 6.1 km s$^{-1}$ 'granitic upper crust' material along each of their profiles, whereas our data show a more rapid increase to higher velocities in southern Afar, leading us to question the degree to which Precambrian basement survives in the axis of the northernmost NMER. Prodehl *et al.* (1997) provide a comprehensive overview and comparative crustal velocity columns of all prior seismic refraction results from the Afro-Arabian rift system, including those north and south of the region discussed in this paper.

Similarly broad-brush estimates of crustal thickness are offered by teleseismic studies and gravity inversions, which are quite compatible with our newer data within their anticipated analytical and interpretational uncertainties. Receiver-function studies (Hebert & Langston 1984; Ayele *et al.* 2004; Dugda *et al.* 2004; Stuart *et al.* 2006) yield estimates of crustal thickness of 27–38 km beneath the NMER, and 33–44 km beneath the eastern and western plateaus. Results from gravity studies (Mahatsente *et al.* 1999; Tiberi *et al.* 2005) suggest that the crustal thickness beneath the Main Ethiopian Rift axis decreases from about 32–33 km in the south to 24 km beneath the southern Afar depression, while thicker crust [*c.* 40 km (Tiberi *et al.* 2005); 38–51 km (Mahatsente *et al.* 1999)] is present beneath the plateau. Tiberi *et al.* (2005) suggest that magmatic underplating may exist beneath several collapsed caldera structures within the rift at around 8° N, 39° W, and Mahatsente *et al.* (1999) predict dense intrusions in both the middle and lower crust beneath the magmatic segments along the axis of the rift.

## EAGLE controlled-source survey

Two *c.* 400 km-long wide-angle reflection/refraction profiles centred on the Boset magmatic segment (Fig. 2), together with a *c.* 100 km-diameter 2D array spanning the rift at the

intersection of the two profiles, were undertaken in January 2003. The NW–SE striking Line 1 was a cross-rift profile extending from the Blue Nile Gorge on the western plateau to the Bale Mountains on the eastern plateau (Fig. 2). The NE–SW striking Line 2 was an along-axis profile, crossing a number of basins from Lake Awassa in the south to Gewane in the north, and also the Gedemsa,

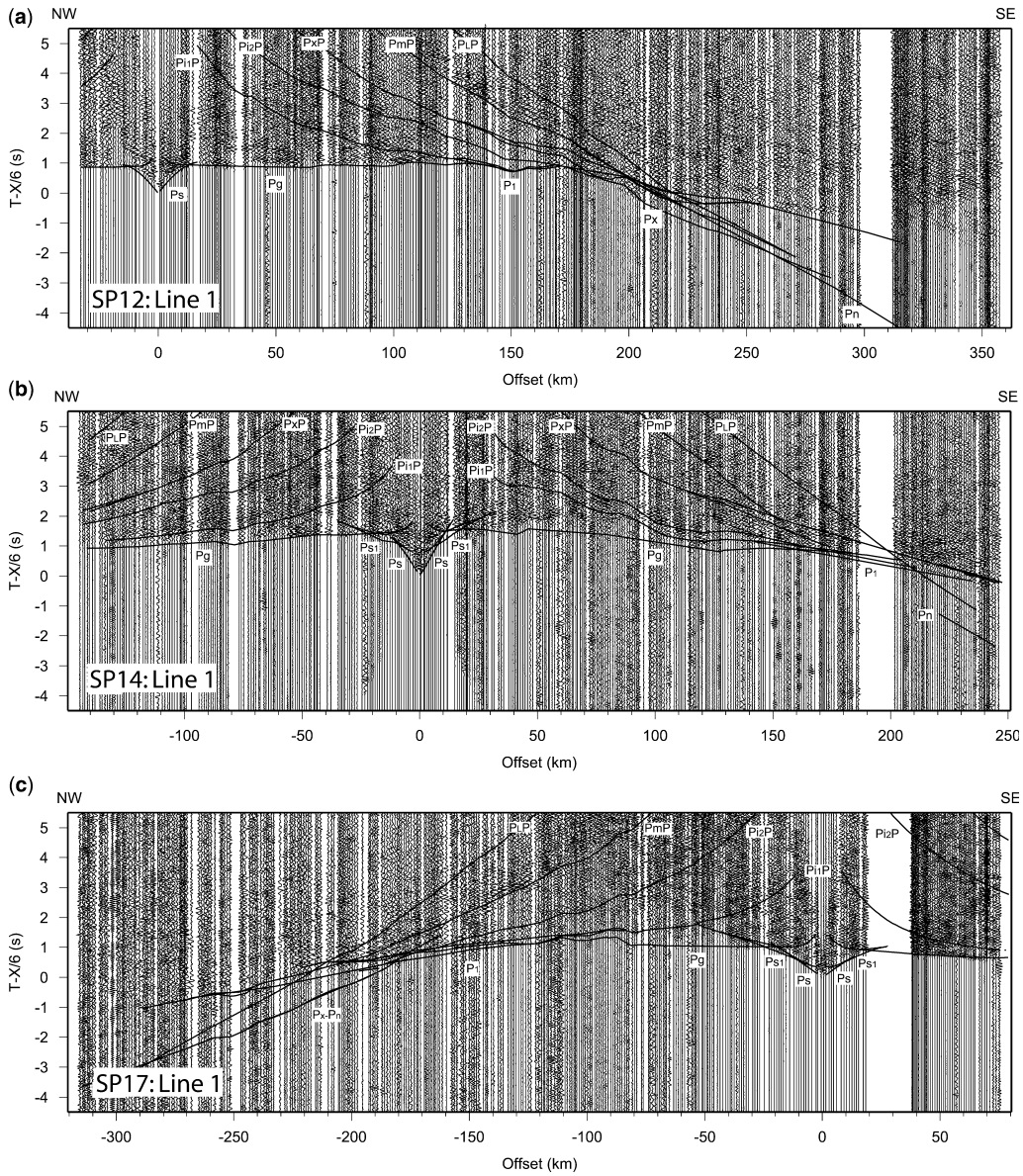


**Fig. 3.** Example seismic record sections from: (a) SP12 – Line 1; (b) SP14 – Line 1; (c) SP17 – Line 1; (d) SP25 – Line 2; (e) SP28 – Line 2. Sections are reduced at 6 km $s^{-1}$ with trace-normalized amplitudes and are bandpass-filtered from 4–16 Hz. Calculated travel-time curves from the velocity model shown in Fig. 5 are overlain. Phase labelling: Ps and $Ps_1$, sedimentary diving waves; Pg, crystalline basement diving wave; $P_1$, diving wave in mid–upper crust; $P_2$, diving wave in lower crust; Px, diving wave in high-velocity lowest crustal layer (HVLC); Pn, mantle diving wave; $Pi_1P$, reflection from mid–upper crust reflector; $Pi_2P$, reflection from top of lower crust; PxP, reflection from top of HVLC layer; PmP, Moho reflection; $P_LP$, mantle reflection.

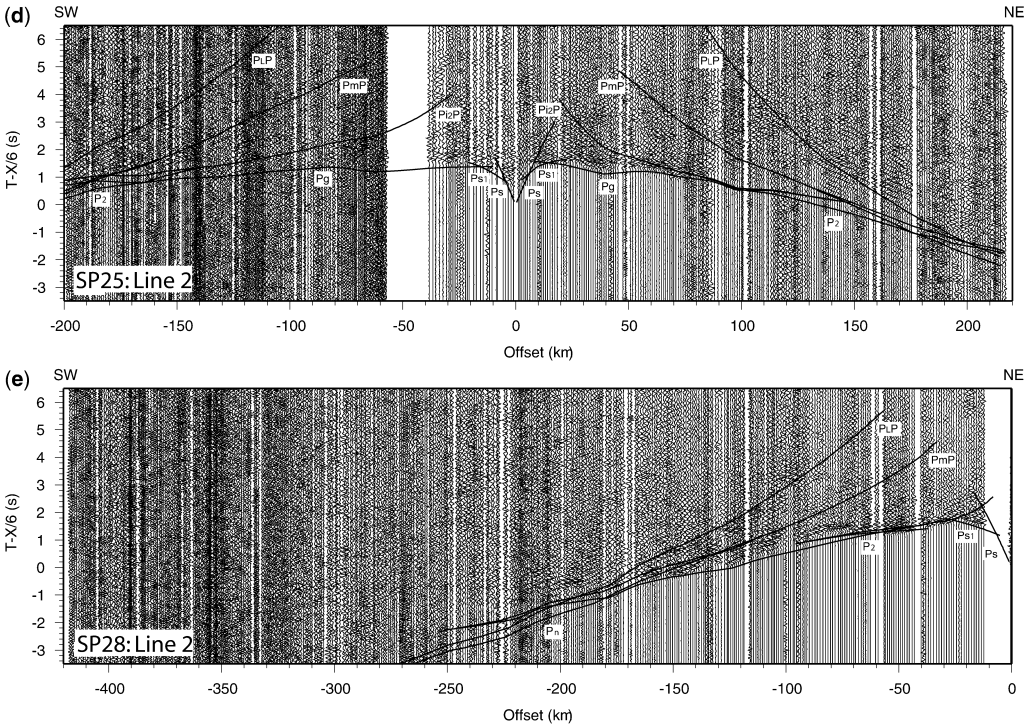


**Fig. 3.** *Continued.*

Boset, Fantale–Dofan and Angelele magmatic segments (Fig. 2). The profiles intersected above the Boset magmatic segment. The 2D array lay substantially within the NMER.

A total of 23 explosive charges ranging from 50 to 5750 kg with an average shot size of 1100 kg were detonated in boreholes up to 50 m deep, two lakes (Shala (SP22) and Arenguarde (SP31)) and two quarries (SP41, SP42) (Fig. 2). Shot spacing along the two profiles was a nominal 50 km, with a number of offline shots to extend the ray path azimuthal coverage into the 2D array. The receiver spacing was approximately 1 km along the two 400 km profiles, and 2.5 km within the 2D array, but only where accessible along the road network. Approximately 1000 Reftek single channel 'Texan' seismographs using 4.5 Hz geophones, together with 93 Guralp 6TD 3-component broadband recorders along Line 1, were distributed in one deployment in order to maximize the number of available seismograms. The EAGLE passive broadband arrays (see Stuart *et al.* 2006; Kendall *et al.* 2006) also recorded the 23 shots. Data were recorded with a sample rate of 100 sps for both instrument types. GPS timing was used throughout, with shot and instrument locations being measured using multiple GPS readings.

## Data

Overall data quality is good; best on Line 1 with substantial energy propagation along the entire length of the profile; variable on Line 2 with the southern half of the profile having to be deployed alongside a main highway, but good to the north; and good on the 2D array, although the larger station spacing on that array (*c.* 2.5 km) limits our ability to correlate phases following the first arrival. Representative examples of the seismic data, displayed in the form of distance versus reduced time record sections, are shown in Fig. 3 for shotpoints SP12, SP14 and SP17 on Line 1 and SP25 and SP28 on Line 2.

Seismic phases that have been identified include two from the sediment–volcanic layers close to and within the rift, Ps and $Ps_1$ (e.g. Fig. 3b–e), whereas only a single such phase is observed from seismic sections derived from shots away from the rift on the plateau (Fig. 3a). On only a few sections can

reflections both from within and from the base of the sediment–volcanic layer be identified (e.g. Fig. 3b).

The upper crust has a velocity of *c.* 6.1 km $s^{-1}$ across the whole study area bar the northeastern end of Line 2, based on a consistent Pg arrival, the refracted wave through the crystalline upper crust. This phase is overtaken on a number of sections on Line 1 by $P_1$, the diving wave from a mid–upper crustal layer (e.g. Fig. 3a–c). This phase is difficult to distinguish from Pg, and is identified as it emerges from the reflection $Pi_1P$ originating from this mid-upper crustal layer boundary. On Line 1, $P_1$ and $Pi_1P$ are not seen from every shotpoint, the causative boundary being identified as an 'intermittent' horizon beneath the profile. These phases are not seen on Line 2. This is possibly due to poorer-quality recordings with lower signal-to-noise ratio, or to the reflector not being present beneath this profile. At extreme wide-angle distances, a strong crustal reflection (e.g. Fig. 3a–c) has been correlated as $Pi_2P$, the reflected phase from the top of a lower-crustal layer. This phase is also identified on Line 2 (Fig. 3d).

A generally strong PmP Moho reflection can be identified on all record sections. Mackenzie *et al.* (2005) describe a weak reflected phase, PxP, preceding the PmP phase on the northwestern side of the rift on Line 1. This is interpreted as originating from the top of a lower crustal high-velocity layer, which gives rise to a diving wave with an apparent velocity of 7.4 km $s^{-1}$(e.g. Fig. 3a). On Line 1, there is a weak, low-amplitude diving wave from below the Moho, Pn with an apparent velocity of 8.05 km $s^{-1}$, which can only be definitely identified emerging from beneath the eastern side of the rift (Fig. 3a,b). From SP17 (Fig. 3c), the diving wave beyond 180 km from the shotpoint is weak, and emerges from within the lower crustal layer identified beneath the northwestern side of the rift. Along the axis of the rift on Line 2, the highest velocity identified is 7.5 km $s^{-1}$, derived from a Pn diving wave in the mantle from the northeasternmost shotpoint, SP28 at Gewane (Fig. 3e). This Pn phase is equivalent to that identified by Berckhemer *et al.* (1975) from this region (Profile II: Fig. 2 inset). Additional processing is underway to attenuate noise, but as yet, no other shotpoint on Line 2 has produced clear Pn arrivals.

Mackenzie *et al.* (2005) describe a weak reflected phase, $P_LP$ from the upper mantle (Fig. 3a–c), which is identified from beneath both the northwestern and southeastern flanks of the rift, and beneath the rift itself on Line 1. An equivalent phase is seen on Line 2 (Fig. 3d,e) occurring at noticeably shorter offset beneath the northeastern end of Line 2 than elsewhere. Phase identification was confirmed through the checking of reciprocal times where possible, which proved especially useful for the weaker phases.

## Modelling and model description

For the data from Lines 1 and 2, our travel-time modelling used a combination of travel-time tomography and forward modelling and inversion with the RAYINVR code of Zelt & Smith (1992). The line lengths are beyond the limit for modelling using a flat Earth approximation, and a local Cartesian coordinate system was defined, and model offsets were calculated within this reference frame. The curvature of the Earth appears as a slight bulge on the resultant profile models (Figs 4 & 5). The local Cartesian coordinate system is centred on a point 4942 m below SP25, a point chosen to give all shot and receiver points positive elevations. Since SP28 has the lowest elevation, it has an elevation of zero in the local Cartesian coordinate system.

Following 2D first-arrival travel-time tomography to obtain preliminary velocities for raytracing, initial models were obtained through trial-and-error forward raytrace modelling to fit the picked travel times using a top-down (layer-stripping) approach. Damped least-squares inversion was then used to minimize the resultant travel-time residuals. For Line 1, the model was modified after qualitative comparison of the record sections with synthetic seismograms using the TRAMP code of Zelt & Forsyth (1994).

Interface depth and layer velocity errors were assessed via selective perturbation of the model parameters. For Line 1, the interface depth errors are $\pm 1$ km for intracrustal layers and $\pm 2$ km for the Moho, and $\pm 0.1$ km $s^{-1}$ for upper crustal velocities and $\pm 0.2$ km $s^{-1}$ for lower crustal velocities (Mackenzie *et al.* 2005). For Line 2, the equivalent errors have not yet been defined, but are likely to be somewhat greater than the Line 1 values. Model resolution for Line 1 was assessed from the number of rays traced for any solution, the RMS travel-time residual and the normalized $\chi^2$ value (Zelt & Forsyth 1994). It has not yet been fully assessed for Line 2. To provide an indication of the model resolution, diagrams of source-to-receiver rays are shown for both Line 1 and Line 2 models (Fig. 4a,b). Rays are only shown in Fig. 4 for source–receiver pairs for which the specific phases were visually identified.

Although elevation variations along the profiles are taken into account, the lateral distribution of the shots and recording stations about the best-fit line through each of the two profiles leads to velocity and depth errors in the final models resulting from the crooked line geometry. Each shot record section is analysed with the seismograms at their

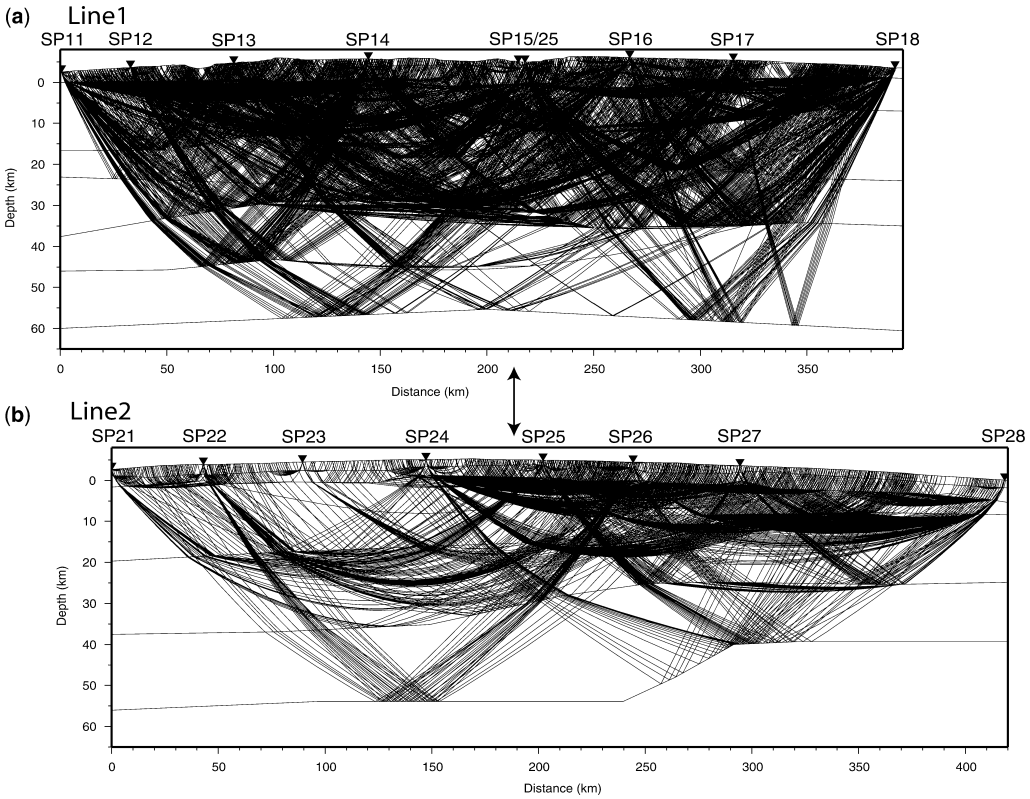


**Fig. 4.** Ray-coverage for Line 1 and Line 2 final models. Lines 1 and 2 are aligned at their intersection (double-headed arrow). RAYINVR (Zelt & Smith 1992) requires layer boundaries to be continuous across the model. Rays are traced from each shotpoint (e.g. SP11) to those recording stations providing phase picks used in the modelling. The low ray-coverage beneath the SW end of Line 2 reflects the poorer-quality data from this region (see text for comment). **(a)** Two-point ray-traced model for Line 1. **(b)** Two-point ray-traced model for Line 2.

true distance from the shot. However, the final 2D model has each shotpoint separated by its true distance from SP11 (for Line 1) and from SP21 (for Line 2). The errors introduced are most severe for large lateral offsets of near-shot stations with respect to the best-fit line through the profile. This situation is common in wide-angle crustal profiling and comment is made only where a noticeable error might be introduced.

The best estimate of the 'cross-over' point for the two profiles is at a distance of 214 km from SP11 and 189 km from SP21 (Fig. 5); the complex geometry is the reason the intersection point on the two lines seems discrepant with respect to SP 15/25. The 2D array data were interpreted using 3D first arrival travel-time tomography (see Keranen *et al.* 2004). Note that the Line 1 and Line 2 modelling procedure utilizes sharp boundaries in seismic velocity (Fig. 5) inferred to represent abrupt lithological changes, whereas the 2D array modelling procedure forces a smoothly varying velocity function (Fig. 6) which is computationally easier to handle in three dimensions.

## *Surface layers*

The surface layer velocities are best defined along the two crustal profiles (Fig. 5). There is a 2–5 km-thick layer of velocity *c.* 5.0 km $s^{-1}$extending the whole length of Line 1. In the central part of the profile, it is covered by a layer of velocity *c.* 3.3 km $s^{-1}$, thickening into the rift. The Line 2 data show that these layers are at least semi-continuous along the rift valley. The total thickness of these layers, which from their velocities are interpreted as sediments and volcanics, appears marginally discrepant at the intersection of the two profiles, being 5.5 km on Line 1 and 4.2 km on Line 2, slightly outside the range of the estimated depth errors. This may be explained by the crooked-line geometry, which produced subsurface ray-paths that do not intersect beneath the

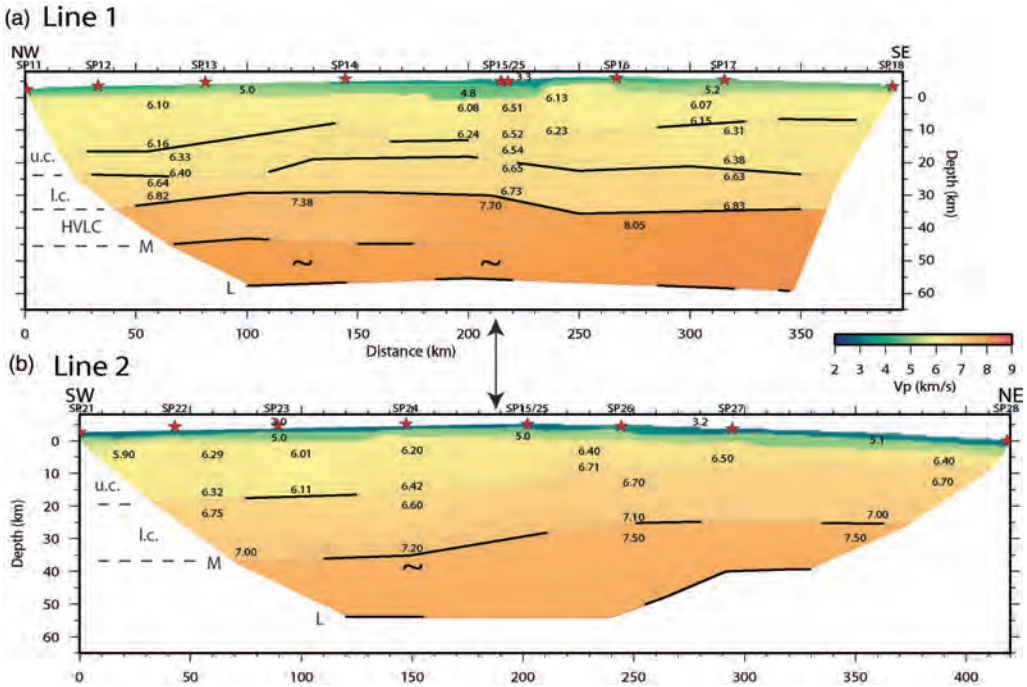


**Fig. 5.** Final ray-trace P-wave velocity models for **(a)** Line 1 and **(b)** Line 2. Model outlines indicate regions sampled by ray-paths (see Fig. 4 for exact coverage). P-wave velocities in km $s^{-1}$. '∼' indicates there is no velocity information available. The depths to the reflectors beneath those regions identified by '∼' have been estimated using laterally extrapolated known velocities within the same layer. Bold lines at layer boundaries are those regions sampled by reflected rays. u.c., upper crust; l.c., lower crust; HVLC, high-velocity lowest crust; M, Moho; L, lithospheric mantle reflector. Lines 1 and 2 are aligned at their intersection (double-headed arrow).

profile intersection at the surface. Given the topographic variations in the region where the lines intersect, the *c.* 50 km distance between shotpoints being of the order of over half the width of the rift valley, the presence of several volcanic centres, and what must be complex shallow subsurface structure that is beyond the resolution of our data, we feel that this tie is as good as one would expect.

## *The crust*

The crustal velocity models beneath Line 1 and Line 2 appear different, in terms of both the numbers of layers and the range of velocities identified at their intersection (Figs 5 & 8). Some differences may be resolved during ongoing modelling of Line 2: to date, the emphasis has been on arrivals that can be correlated along at least most of the profile. However, the strong three-dimensionality of the crust in the NMER (Fig. 6), and the refraction-profiling geometry that dictates that velocities beneath the profile intersection are obtained from quite different shotpoints along each profile, means that it would be a mistake to expect complete agreement. Nonetheless, we restrict our interpretations to the main crustal layers as discussed below.

A brief description of the crustal layering is as follows: beneath both controlled-source profiles, the crust can be divided into an upper crust with velocities of 6.1–6.4 km $s^{-1}$ above a lower crust of velocity *c.* 6.7 km $s^{-1}$ along Line 1, but which includes higher velocities (to 7.1 km $s^{-1}$) beneath Line 2. Beneath Line 1, the upper crust includes high velocities (*c.* 6.5 km $s^{-1}$) beneath a narrow 20–30 km-wide section beneath the rift valley; such velocities are also seen in the upper crust beneath the northern half of Line 2 (Fig. 5) and are resolved into discrete bodies in our 3D analysis (Fig. 6). Beneath Line 1, we identify an intra–upper crustal reflector that may, or may not be continuous across the rift. An anomalous high-velocity (7.4 km $s^{-1}$) lowermost crust has been identified beneath the *c.* 6.7 km $s^{-1}$ layer beneath the northwestern portion of the plateau on Line 1, terminating to the SE in the vicinity of the rift.

The principal observations are as follows:

(1) There is evidence of a high-velocity zone in the upper crust beneath the axis of the rift on

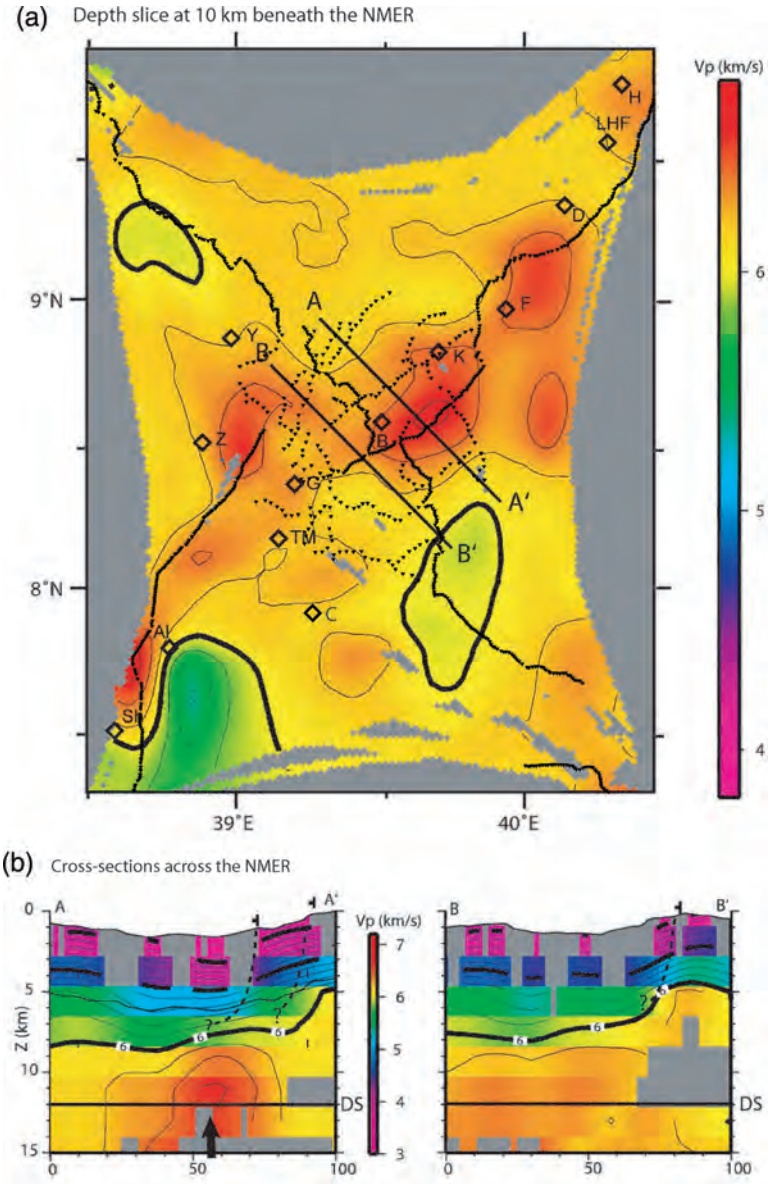


**Fig. 6.** Horizontal slice 10 km below the surface beneath the 2D array. The final model has been smoothed over a $6 \times 6 \times 2$ km (xyz) spatial node and a 2 km velocity node distribution. Receiver positions (EAGLE Lines 1 & 2 and 2D array) shown by inverted triangles. Thick contour line marks 6.0 km $s^{-1}$ with minor contours at 0.2 km $s^{-1}$ intervals. High-velocity bodies (red) interpreted as solidified magmatic intrusions beneath the rift floor. Sections AA′ and BB′ displayed in Figure 6b. Diamonds identify volcanoes. Along the rift axis from south to north are: Sh, Shala, Al, Aluto, TM, Tullu Moje, G, Gedemsa, B, Boset, K, Kone, F, Fantale, D, Dofan, LHF, Liado Hayk Field, and H, Hertale. On the rift flanks are C, Chilalo, Y, Yerer, and Z, Zikwala (after Keranen *et al.* 2004 (reproduced with permission of the Geological Society of America)). (**b**) Rift-perpendicular cross-section AA′ extending through the Boset magmatic segment between Boset and Kone volcanoes. Model smoothing as for Figure 6a. The thick contour line at 6.0 km $s^{-1}$ is identified with other contours at 0.2 km $s^{-1}$ intervals. High-velocity ($V_p$) body (vertical arrow) beneath rift valley is interpreted as solidified mafic intrusion into Precambrian basement. Fault symbols and proposed subsurface continuation of faults (dashed lines) are marked. Depth of slice in Figure 6a is marked by horizontal line. Areas with no ray coverage are shown in grey. BB′ shows rift-perpendicular section between magmatic segments (after Keranen *et al.* 2004 (reproduced with permission of the Geological Society of America)).

Line 1, with velocities of *c.* 6.5 km s$^{-1}$. Similar velocities identified in the crustal model derived from the 2D array (Fig. 6) lie beneath the Boset magmatic segment. There is an equivalent velocity anomaly identified on Line 2, but slightly displaced to the NE from the cross-over of the two profiles. This would be expected from the 'wiggly' nature of Line 2, in particular in the vicinity of the Boset magmatic segment. The results from the 2D array (Keranen *et al.* 2004), which take full account of the nature of the subsurface and array geometry, definitely show that there is more than one such high-velocity zone and that these are segmented along the axis of the rift (e.g. as shown at 10 km depth below the surface in Fig. 6a).

(2) The upper crustal layer beneath Line 1 ($V_p$ 6.1–6.4 km s$^{-1}$) is about 28 km thick beneath the plateau on both sides of the rift valley (Fig. 5a). Immediately beneath the rift, and for about 40 km to the NW, the upper crust appears to thin to 23 km along Line 1. Beneath the rift along Line 2, the upper-crustal thickness decreases slowly northwards from SP22 (20 km) to SP 24 (18 km). It then thins dramatically across a 50 km-long zone in the region of the Boset magmatic segment to become only about 8 km thick beneath the northern part of Line 2 (Fig. 5b). There is a difference of only 4 km in the estimated depth to the base of the upper crust at the Line 1/Line 2 intersection, which we believe is acceptable given the rapid change in the depth of this layer near the intersection and the complexities present in this area.

(3) The upper crustal layer ($V_p$ 6.1–6.4 km s$^{-1}$) on Line 1 contains an intralayer reflection which may or may not be continuous along the profile. This reflector shallows from 20 km depth beneath the surface to the NW of the rift, to 12 km beneath the surface to the SE. Another intracrustal reflector is also modelled on the same profile beneath the rift axis. It is unclear whether these reflectors are continuous. No such reflector can be positively identified along the axis of the rift, but the lower data quality along Line 2 may preclude identification of a weak reflection resulting from such a boundary.

(4) The lower crust ($V_p$ 6.6–7.1 km s$^{-1}$) on Line 1 appears to change in thickness from 14 km beneath the eastern plateau to 9–12 km beneath the northwestern end of the profile where it overlies an anomalous layer of velocity 7.4 km s$^{-1}$ described below. There is no obvious change in thickness of the lower crustal layer immediately beneath the rift along Line 1, and its thickness is also relatively uniform at 16–20 km along the length of Line 2. While the velocity errors on Line 2 are not yet well defined, there may be an apparent correlation between the variation in velocity observed in the lower crust and that identified in the upper crust (Fig. 5b). The topmost lower crust velocity peaks at about 6.75 km s$^{-1}$ at 50 km from SP21, 6.9 km s$^{-1}$ at 215 km from SP21, and at 6.8 km s$^{-1}$at 300 km from SP21, each location being beneath a velocity 'high' in the upper crust.

### *Upper mantle and anomalous lower crust*

Beneath the southeastern flank of the rift, a normal mantle (P-wave velocity 8.05 km s$^{-1}$) underlies the lower crust at a depth of *c.* 40 km. Beneath the axis of the rift on Line 1, the velocity drops to 7.7 km s$^{-1}$, consistent with the along-axis velocity of 7.5 km s$^{-1}$ observed on Line 2 (as yet derived primarily from a diving phase from SP28 (Fig. 2)). The crust thins from about 40 km in the SW to 26 km in the NE beneath Line 2, with a consistent estimate of around 35 km beneath the intersection of the two profiles.

The most 'anomalous' layer in the derived model underlies the plateau NW of the rift on Line 1. Here, a 15 km-thick layer of P-wave velocity 7.4 km s$^{-1}$ lies at a depth of approximately 33 km (HVLC in Fig. 5a). It is defined by reflections from its top and base. There is no velocity estimate for the material underlying it, but it cannot be more than 8.0 km s$^{-1}$ otherwise it would have produced a first arrival diving wave, which is not observed. The depth (*c.* 48 km beneath the surface) to the base of this layer is significantly greater than the Moho depth beneath the eastern flank of the rift. The location of the layer underlies thinned lower crust beneath the northwestern flank of the rift (Fig. 5a).

There are distinct variations in the characteristics of the Moho reflections (PmP) identified on the cross-rift profile Line 1 (Fig. 7). From 90–130 km NW of SP18, PmP with bounce points beneath the southeastern margin of the rift is a simple phase with clear low-frequency content (Fig. 7c). Between offsets of 90–150 km from SP17, PmP with bounce points beneath the rift has a variable-amplitude, higher frequency, very reverberative character (Fig. 7b). Such reverberative characteristics are also identified from PmP reflections with bounce points beneath the northwestern margin of the rift between 110–150 km from SP12 (Fig. 7a). These reverberations occur behind the onset of the phase originating from the base of the 7.4 km s$^{-1}$

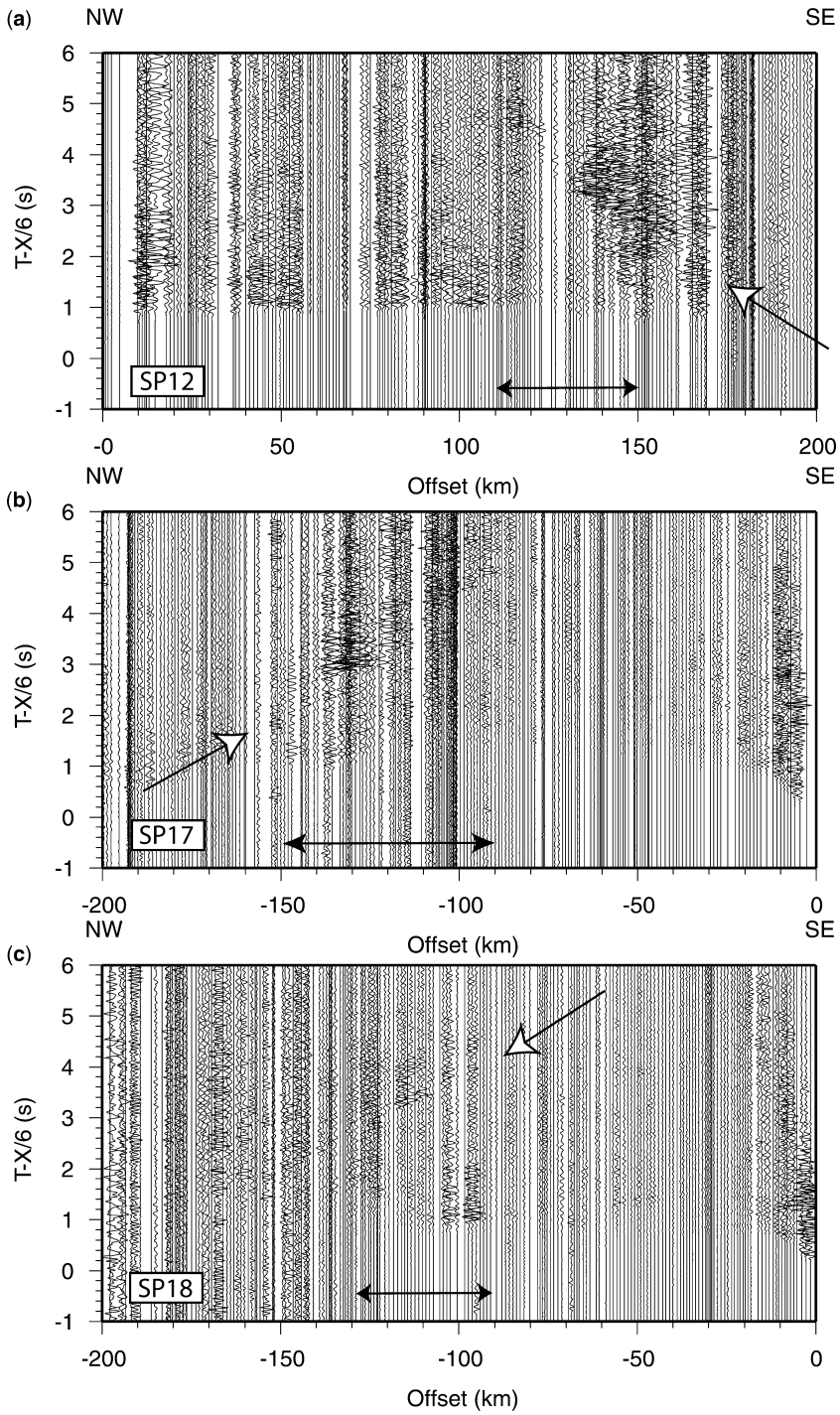


**Fig. 7.** Variability of PmP phase (identified by open-ended arrow) occurring between *c.* 2 to 5 seconds reduced time and offsets marked by arrows. Display parameters as for Fig. 3. **(a)** SP12 – Line 1 (strong reverberation between 110–150 km offset); **(b)** SP17 – Line 1 (strong reverberation between 90–150 km offset); **(c)** SP18 – Line 1 (non-reverberative phase between 90–130 km offset).

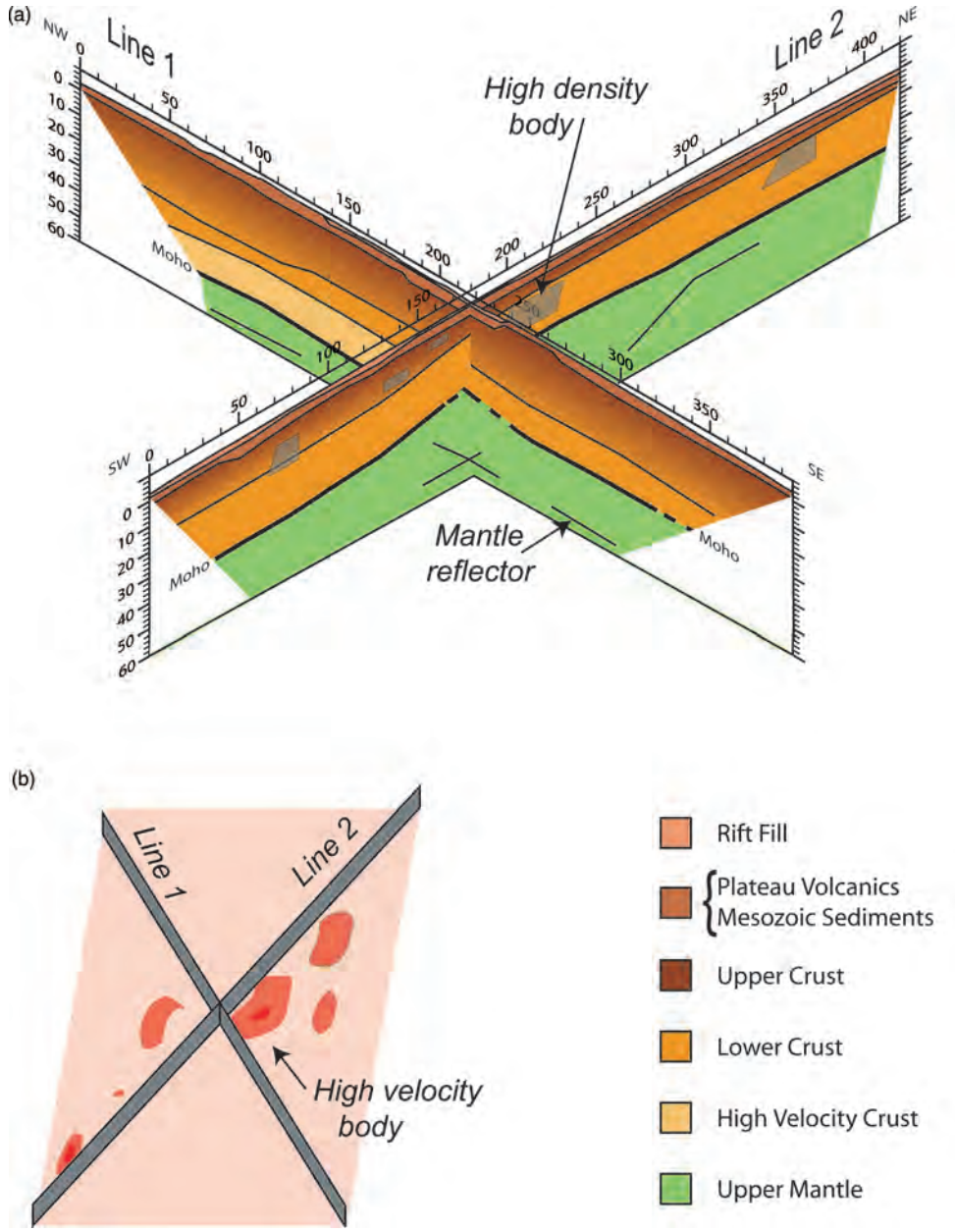


**Fig. 8.** Cartoon depicting two 3D views of the controlled source seismic results; A – from a southerly elevation; B – from a near vertical elevation. Lines 1 and 2 form a fence diagram. Red polygons are areas of seismic velocity higher than 7 km.s$^{-1}$ from Figure 6a projected onto a horizontal plane at 10 km depth. Grey polygons are mafic bodies with density $\sim 3000$ kg.m$^{-3}$ projected onto a vertical plane along the NE-SW axis that is Line 2..

layer, suggesting that it is this layer that is producing them.

On a number of the shotpoint record sections, there is also a reverberative reflection that occurs beneath the Moho. Although its depth cannot be defined precisely owing to the limited data constraining sub-Moho velocities, it can be identified not only beneath the eastern and western margins

of the rift but also beneath the rift itself, where it may be slightly shallower than beneath the rift flanks (Fig. 5a). Below Line 2, where it is sampled beneath two regions, the same reflector is about 60 km beneath the southern part of the profile, and about 40 km beneath the northern part (Fig. 5b); thus its depth appears to correlate with crustal thickness.

## Interpretation

The layer thicknesses and velocities derived from the EAGLE controlled-source data confirm that the crust beneath the Main Ethiopian Rift is still predominantly continental in nature, with the principal modifications being: high-velocity intrusions segmented along the axis of the rift; alteration to a massively intruded, thinned crust in the southwest corner of Afar; and the presence of an anomalous 'underplate' layer beneath the plateau northwest of the rift. This crust overlies a mantle which appears normal beneath the southeastern part of Line 1 but modified by thermal processes elsewhere, and which includes a prominent reflector 10–20 km below the Moho along and adjacent to the rift.

### *Sediments and volcanics*

The near-surface sedimentary and volcanic layer of velocity *c.* 5.0 km $s^{-1}$ that is continuous along the length of both Line 1 and Line 2 most likely represents a combination of Mesozoic sediments and Oligocene flood basalts. In the central part of Line 1 and along Line 2, the lower-velocity overlying layer, thickening into the rift, correlates with the distribution of both the Quaternary sediments and the Pliocene–Miocene basalt and ignimbrite units associated with the early stages of extension in the NMER (Wolfenden *et al.* 2004). The thickening of these sedimentary–volcanic layers both on the cross-rift profile (Line 1) and beneath the 2D array (Fig. 6b) into the Arboye border fault (Fig. 2) of the Adama basin is consistent with structural studies (Wolfenden *et al.* 2004). This suggests that the varying thickness of the equivalent layers along Line 2 may result from this profile overlying other structural sub-basins along its length. The thickness of these layers along Line 2 only varies significantly in a few places, perhaps because the recording profile followed roads in physiographic lows that are also structural lows, so that a relatively uniform basement depth is detected. Alternatively, it may be because rift formation in the NMER has indeed created only limited along-axis basement structural variations, but this seems unlikely based on results from many other rifts. There is also significant basement topography to the SE of the rift on Line 1 near SP16 that does not correlate with surface topography and may result from Mesozoic extension (Korme *et al.* 2004)

### *Upper-crustal magmatic segmentation*

The P-wave velocity of *c.* 6.1 km $s^{-1}$ beneath the sedimentary–volcanic layer on Line 1 and the southern part of Line 2 is consistent with the presence of Precambrian crystalline basement. The high velocity of *c.* 6.5 km $s^{-1}$ beneath the axis of the rift on Line 1, highlighted in the 3D crustal model derived from the 2D array (Fig. 6) and lying beneath the Boset magmatic segment, suggests the presence of a gabbroic magmatic intrusion based on these velocities and the modelled density of 3000 kg·$m^{-3}$ (Cornwell *et al.* 2006; Mahatsente *et al.* 1999). Keranen *et al.* (2004) discuss the along-axis segmentation of these high-velocity zones (Fig. 6a) and their correlation with the positions of the Quaternary magmatic segments arranged en echelon along the rift. These results together with examination of the Line 2 upper-crustal layer show that such high-velocity zones can be identified in particular beneath the Lake Shala caldera, the Gedemsa magmatic segment, the northern end of the Boset and the southern end of the Fantale–Dofan magmatic segments. Interestingly, the Boset magmatic segment and those to the NE appear slightly offset to the SE of the high-velocity zones, while those magmatic segments to the SW of Boset appear offset to the NW of the high-velocity zones (Fig. 6a).

### *Along-axis crustal thinning*

The thinning of the upper crust beneath the northern part of Line 2 is consistent with previous results from the area (Berckhemer *et al.* 1975; Makris & Ginzburg 1987). We infer significant extension of the brittle upper crust, whereas the lower crust of relatively uniform thickness along the axis of the NMER is at first sight unaffected. Previous authors (e.g. Makris & Ginzburg 1987) have suggested that this lower crustal layer may have been significantly intruded by mafic material beneath southwestern Afar, so masking crustal stretching. The velocity of this layer (*c.* 6.9 km $s^{-1}$), though variable, does not change significantly between the southern and northern parts of Line 2. This might suggest there is little petrological difference between the highly extended region at the northeastern end of the profile in southwestern Afar and the less-extended region to the SE. However, significant elevation of the geotherm in southwestern Afar would result in a lowering of velocity, which would then suggest

the presence of more mafic intrusive material in the lower crust beneath Afar than further to the SW.

### *Upper mantle beneath the NMER*

There is normal mantle of P-wave velocity 8.05 km $s^{-1}$ beneath the southeastern flank of the rift identified beneath Line 1. The sub-Moho Pn mantle diving wave velocity of 7.7 km $s^{-1}$ modelled beneath the rift axis on Line 1, and the equivalent velocity seen at the same boundary along the axis of the rift, is similar to that identified beneath the axis of the Eastern (Kenya) Rift (Mechie *et al.* 1994*a*). In Kenya, such a mantle velocity has been interpreted from the joint analysis of seismic velocities and xenolith compositions (Mechie *et al.* 1994*b*) to result from 3–5% partial melt trapped in the mantle. This would be consistent with Bastow *et al.*'s (2005) conclusions that upper mantle low-velocity zones beneath the NMER result from anomalously high temperatures and local areas of melting or melt-ponding. EAGLE shear-wave splitting data also indicates partial melt in the upper mantle and crust beneath the rift axis (Kendall *et al.* 2005; Keir *et al.* 2005).

The upper mantle reflector at a depth of about 60 km beneath the rift valley and its flanks, and identified at 40 km beneath southwestern Afar, is discussed separately below.

### *Anomalous lower crust*

If taken at face value, the anomalous lower crust ($V_p$ 7.4 km $s^{-1}$) beneath the northwestern part of Line 1 merges with a higher-velocity upper mantle layer under the rift valley region. However, we feel confident that this is an artefact of the modelling algorithm that requires interfaces to be continuous across the model. In the NW where it is part of the crust, this layer is characterized by a distinct reflection from its base, whereas there is no equivalent reflection from the *c.* 7.5–7.7 km $s^{-1}$ layer below the rift axis and above the mantle reflector at 60 km (which is also observed beneath the anomalous crustal layer). We therefore suggest this anomalous lower crustal layer terminates at or near the rift's western escarpment but could have extended across at least some of the rift valley region before the recent extension and magmatism. To the NW, this layer appears reverberative in the seismic sections (Fig. 7a), and forward modelling of Line 1 gravity data is also consistent with its presence (Cornwell *et al.* 2006). The lateral extent of this layer under the plateau may perhaps be limited, because Berckhemer *et al.* (1975) and Makris & Ginzburg (1987) did not identify a layer with *c.* 7.5 km $s^{-1}$ velocity beneath their Profile 1 (inset to Fig. 2), and their estimate of depth to 'normal mantle' beneath the plateau is equivalent to the base of our anomalous layer beneath Line 1.

However, one may question whether the 1972 refraction data truly have the resolution to recognize the high-velocity lower crust. Stuart *et al.* (2006) incorporating results from a previous survey (Dugda *et al.* 2004) use receiver functions to derive crustal thickness and average $V_p/V_s$ estimates over the NMER and its flanking plateaus. Their thickness estimates derived from both within the NMER and on its southern margin are consistent with those derived from the controlled-source study. However, those obtained from stations close to or coincident with the northwestern end of Line 1 on the plateau, have apparently identified the top rather than the base of the anomalous crustal layer. This discrepancy is discussed in detail in Stuart *et al.* (2006). It may in part be due to the different signal characteristics (wave-type, wave-length, spatial sampling, ray-path orientation) used by the receiver function method and wide-angle controlled-source analysis procedures. However, the complex lower crust/upper mantle structure in the vicinity of this anomalous lower crustal layer may also be a contributory factor. It is therefore apparently not possible at present to constrain the areal extent of this anomalous underplate layer.

Mackenzie *et al.* (2005) argue that the anomalous layer under the plateau NW of the rift valley is equivalent to a magmatic underplate layer that is characteristic of continental volcanic margins (e.g. Kelemen & Holbrook 1995; Menzies *et al.* 2002). The existence of the layer beneath the northwestern plateau, where the maximum thickness of flood basalts is observed, suggests a direct connection to the Oligocene volcanics. Such a link would imply uplift of the plateau associated with the emplacement of the flood basalts, consistent with the initiation of the Blue Nile canyon at 25–29 Ma (Pik *et al.* 2003) and with geochemical studies of the Oligocene plateau rhyolitic ignimbrites which originate from the fractional crystallization of $\geq$3 km of gabbroic underplate (Ayalew *et al.* 2002). The recent felsic magmatism may also have been generated from partial melting of existing gabbroic underplate followed by fractionation at upper crustal levels (Trua *et al.* 1999; Ayalew *et al.* 2006). As stated above, there is significant reverberative seismic energy originating within this anomalous lower crustal layer, which may be consistent with the presence of layering within underplated material (e.g. Deemer & Hurich 1994). We therefore suggest that this layer results from magmatic addition to the base of the crust, initially emplaced in the Oligocene, but with a likely recent component derived from the conduit of hot rising material observed in the

mantle to the NW of the rift beneath Line 1 (Bastow *et al.* 2005). The emplacement of this underplate, whether Oligocene or recent, at the base of the crust, would have resulted in melting and assimilation of pre-existing lower crust, potentially explaining slight thinning of the lower crust above the anomalous layer. We interpret the upper surface of the anomalous lower crust as the relict Moho prior to plume impingement beneath Ethiopia, being at an equivalent level to the Moho SE of the rift, and as a passive strain marker for subsequent extension across the rift (see below).

## Discussion

### *Magmatic segments*

There is a direct spatial correlation between the surface magmatic segments along the axis of the rift and the 20 km-wide, 50 km-long high-velocity zones identified within the upper crust from the controlled source study (Fig. 6a). This correlation, the high-velocity bodies and the magmatic segments being arranged en echelon along the rift axis, but slightly offset in different senses to the north and south of Boset, strongly implies a causative link. Keranen *et al.* (2004) interpret the high-velocity bodies in terms of cooled gabbroic intrusions accommodating extension at mid-crustal levels. They state there is no marked increase in velocity at shallow depths beneath the surface magmatic segments, suggesting that dykes can only contribute to about 30% of the equivalent extension in the brittle upper crust, the remainder being accommodated by recent dense faulting. NMER seismicity shows a concentration of low-magnitude earthquake swarms at the base of the 6–9 km deep seismogenic layer beneath the magmatic segments (Keir *et al.* 2006) coincident with the top of the zone of extensive mafic intrusions imaged at 7–10 km depth (Fig. 6) (Keranen *et al.* 2004) and also observed below Line 1 (Mackenzie *et al.* 2005). This is consistent with extension above and below the mid-crustal mafic intrusions being accommodated seismically and aseismically respectively (Keir *et al.* 2006; Bendick *et al.* 2006). The small offset of the surface magmatic segments with respect to the high-velocity bodies at depth may result from the basaltic lavas reaching near-surface magma chambers having to 'by-pass' the cooled, rigid gabbroic intrusions at mid-crustal levels, the path of least resistance to the surface being up the side of the gabbroic bodies.

The EAGLE controlled-source project has imaged the main border fault on the southeastern side of the rift (Mackenzie *et al.* 2005; Keranen *et al.* 2004) at 235 km from SP11 (Fig. 5a). Keranen *et al.* (2004) state that the low-velocity near-surface section seen in the 3D model is offset by a subsurface continuation of the Asela (Sire) border fault (Fig. 2), which overlies a high-velocity mid-crustal magmatic intrusion (Fig. 6a). They also show a section across the rift between magmatic segments (Fig. 6b) in which the border fault is also imaged, although a magmatic intrusion is not, which demonstrates support for previous observations that magmatic and structural segmentation of along-axis rift basins are not well correlated (Ebinger & Casey 2001).

The strong reverberatory nature of the Moho reflection from beneath the Boset magmatic segment on Line 1 (Fig. 7b) and the lack of an equivalent signature on the reflection from beneath the southeastern flank of the rift provides a similar relationship to those seen on seismic record sections obtained across the eastern (Kenya) rift. There, reflectivity modelling suggested that the most likely cause of such reverberations resulted from intrusions within the lowermost crust beneath the rift (Thybo *et al.* 2000). Assuming it results from a similar cause beneath Line 1, this reverberatory signature provides evidence for magmatic alteration of the lower crust beneath the Boset magmatic segment. The possible correlation between the high-velocity upper-crustal bodies along the axis of the rift and the along-axis variation in velocities in the lower crust would imply that the magmatic segmentation that is observed on the surface and linked to that identified in the upper crust, also exists in the lower crust. Bastow *et al.* (2005) propose that along the rift axis the segmentation of the low-velocity mantle upwelling beneath the rift is controlled by the mechanically segmented early continental rift structure and that this focuses melt along the rift axis. Keir *et al.* (2006) discuss the possible linkage between magma source regions and surface magmatic segments, commenting on SKS shear-wave splitting studies of lithospheric anisotropy which is likely due to vertically-oriented dykes including partial melt that cross-cut the lithosphere (Kendall *et al.* 2005). Exactly how the melt might then be distributed into the pattern of magmatic segmentation (that is not well-correlated with the early rift structural segmentation) is yet to be resolved, although our results show that this distribution has definitely occurred by the time the melt has reached mid-crustal, and probably lower-crustal levels.

### *Crustal extension*

It would be expected that extension across the rift has been accommodated by faulting and dyking in the brittle upper crust, and ductile flow and

magmatic intrusion within the lower crust. Estimates of extension across the rift are complicated by the presence of the Oligocene underplate that has almost certainly eroded or added to the crust beneath the northwestern plateau but by unknown amounts. If we assume that crustal thickness beneath the basement surface was uniform across the rift and equivalent to that identified beneath the southeastern margin (35 km), the present crustal thickness beneath the basement surface below the rift itself (27 km) results in a stretching factor of about 1.3 on Line 1. The intersection point of the two EAGLE profiles lies over the marked decrease in crustal thickness from south to north along the axis of the rift. The crustal thicknesses beneath the basement surface at the south (33 km) and north (21 km) ends of the along-axis profile, Line 2, result in stretching factors of 1.1 and *c*. 1.7 within the Main Ethiopian Rift and in southwestern Afar to the south of Gewane respectively (Fig. 2). These figures correspond with those derived from a recent gravity analysis of 1.2 and 2.0 in the central MER and within the Afar depression to the north of Gewane respectively (Tiberi *et al.* 2005). Eagles *et al.* (2002), from a study of the kinematics of the Danakil microplate, suggest recent extension rates in central and southern Afar are low, being $2-3.5\ \mathrm{mm\ a^{-1}}$ respectively, and Wolfenden *et al.* (2004) arrived at a similar value for the northern MER. Eagles *et al.* (2002) estimate that the crustal stretching factor is $>3$ in central and southern Afar. The high velocities obtained within the upper crust beneath the rift identified from all the controlled source studies have been interpreted in terms of mafic intrusions beneath the surface magmatic segments. The presence of these intrusions, together with likely associated underplating/intrusion at the base of the crust, will result in our extension factors being underestimations.

While the variation in cross-rift crustal velocities would suggest that modification of the crust has primarily occurred beneath the rift itself, the variation in depth to the upper–lower crust boundary (22–27 km) beneath Line 1 indicates that the upper crust has been thinned over a wider (*c.* 100 km) zone extending to the NW beneath the plateau.

Following primary rift development in the NMER after 11 Ma, there was a hiatus in volcanic activity between 6.5 and 3.2 Ma after which deformation migrated to a narrow zone in the rift centre (Wolfenden *et al.* 2004). Keranen *et al.* (2004), using results from the 2D array data that are consistent with those from Line 1 (Mackenzie *et al.* 2005), state that the *c.* 20 km-wide mafic intrusions in the mid-crust beneath the rift are compatible with the 27 km of extension predicted in the last 3.2 Ma. from plate motions (Horner-Johnston *et al.* 2003). They also suggest that above these intrusions, the maximum estimate of mafic material in the upper crust is about 30% of the 20 km-wide dyke-bearing segments, the remaining extension being taken up by faulting localized to the narrow 20 km-wide segments within the rift. Assuming the width of the extended zone is roughly 100 km as derived from the thinned upper crust across the rift, an overall stretching factor of 1.3 would imply that the amount of extension prior to the migration of deformation at around 3.2 Ma towards the centre of the NMER was about 10 km.

One of the most significant results from our controlled-source survey is the decrease in crustal thickness along Line 2 from south to north into Afar. The degree of extension increases markedly towards Afar. Hypotheses based on the difference in amount of thinning between the upper and lower crustal layers beneath the northeastern end of Line 2 are difficult to test. This results from the difficulty of interpreting seismic models in regions affected by significant magmatic intrusion, owing to the tendency of low-velocity crustal material to be overprinted by higher-velocity material as a result of mafic intrusion. It is possible the mid-crustal layer boundary at the northern end of Line 2 identifies the top of these intrusives, which have penetrated the upper crust.

However, analysis of the crustal velocities and layer thicknesses along this profile might suggest that continental extension (with relatively high crustal velocities associated with the magmatic segments at the southern end of the profile) apparently passes through a transition between SP15/25 and SP27 into near pure spreading at the northern end of the profile. The results from our study, together with those of Berckhemer *et al.* (1975), Makris & Ginzburg (1987), Tiberi *et al.* (2005) and Stuart *et al.* (2006), all indicate an increase in the amount of intrusive material in the crust beneath southwestern Afar. Stuart *et al.* (2006) also show that, within the rift, the $V_p/V_s$ ratio increases to greater than 2.0 (Poisson's ratio, $\sigma > 0.33$) northwards towards the Afar depression, being indicative of partial melt in the crust. Bastow *et al.* (2005), using the methods of Gao *et al.* (2004) to relate seismic-velocity variations to temperature, suggest that lateral variations of between roughly 125 to 800 °C are present beneath the study region if the velocity variations are attributed solely to temperature effects. However, from examination of P and S relative arrival time residuals, they show that the values imply the presence of partial melt, especially beneath the rift, consistent with the predictions of Kendall *et al.* (2005) from analysis of SKS shear-wave splitting observations across the EAGLE network. Melt reduces the temperature contrasts necessary to explain the low velocity anomalies.

If the excess mantle temperature were of the order of 400 °C, this coupled with a stretching factor of 2 derived for the northern end of Line 2 would suggest about 20 km of the present crustal thickness could have resulted from melt produced from adiabatic decompression alone (e.g. White & McKenzie 1995). However, with the excess temperature not being defined, exact determination of the melt fraction within the crust beneath southwestern Afar is beyond the scope of this review. It should be noted that Eagles *et al.* (2002) suggest the possibility of presently active sea-floor spreading in central and southern Afar.

The recent focusing of faulting and intrusion of mafic material towards the axis of the rift, the increased amount of mafic intrusion with increased amount of extension from south to north along the axis of the NMER, the link between crustal magmatic processes and the deeper low-velocity mantle zones interpreted in terms of high temperatures and the presence of partial melt are all consistent with the magma-assisted rifting hypothesis of Buck (2004) as discussed in other EAGLE publications (e.g. Bastow *et al.* 2005; Stuart *et al.* 2006; Kendall *et al.* 2005, 2006).

### *Implications of the underplated lower crust*

The presence of thick, high-velocity crust under the Ethiopian plateau NW of the rift raises several questions. The first is simply its origin, and Mackenzie *et al.* (2005) argue that this layer is due to underplating that was initiated during the 31–29 Ma flood basalt event. Underplating can be the result of a number of magmatic processes, but the end result is thickening of the crust, which from a simple Airy isostasy viewpoint would cause uplift. The Ethiopian plateau (Fig. 2) has an excess elevation above the mean continental elevation of up to approximately 2 km (e.g. Nyblade & Sleep 2003).

Thus, the question arises, how much of this uplift is a result of the underplating? Based on its velocity of 7.4–7.7 $km/s^{-1}$, compared to a mantle velocity of 8.05 $km/s^{-1}$ (Fig. 5), the 15 km-thick lens of underplate at the base of the crust beneath Line 1 has a density contrast with the upper mantle of 125 to 230 kg $m^{-3}$ (Brocher 2005), yielding a permanent isostatic uplift of 0.6 to 1.0 km. New gravity modelling, based on our Line 1 refraction data, corroborate this expected density contrast (Cornwell *et al.* 2006) and hence the expected uplift due to underplating. This indicates that the elevation of the plateau must be supported in part by the buoyancy of the mantle. Impingement of the plume head beneath Ethiopia would have produced a transient dynamic uplift up to *c*. 500 m but this would have decayed to less than half its initial value in the 30 Ma that have elapsed since (Nyblade & Sleep 2003). If the permanent uplift due to underplating and lingering dynamic effects of the plume total only around 1 km, the remaining excess elevation must be due to regional mantle density contrasts.

The tomographic results of Bastow *et al.* (2005) document that relatively low seismic velocities in the upper mantle extend west from the Main Ethiopian Rift under the plateau and also extend to considerable depth (>100 km). The lowest velocities are of limited lateral extent under the plateau, but even a small density contrast of 50 kg $m^{-3}$ extending to 10 km could produce the needed 1 km of uplift. Although the EAGLE mantle tomography (Bastow *et al.* 2005) and even the broader study of Benoit *et al.* (2006) are too spatially limited to properly demonstrate that mantle velocities beneath the plateau are lower than beyond the plateau, the implication of our EAGLE refraction study which finds insufficient underplating to explain the observed uplift is that mantle densities (hence velocities) beneath the plateau must be lower than beneath surrounding areas, as shown by Cornwell *et al.* (2006). This result echoes the recognition of different upper-mantle structure beneath the rifts and shields further south in East Africa (e.g. Nyblade 2002).

### *The mantle reflector*

The mantle reflector identified beneath both Line 1 and Line 2 was also observed beneath the previous controlled-source profiles beneath Afar (Berckhemer *et al.* 1975; Makris & Ginzburg 1987). Interestingly, a similar feature was identified beneath all of the KRISP seismic profiles in Kenya (Keller *et al.* 1994; Maguire *et al.* 1994; Prodehl *et al.* 1994; Byrne *et al.* 1997). The distinctive features of the reflector are that it exists at a depth of approximately 10–25 km beneath the Moho. The northern extent of the KRISP 90 along-axis profile (Keller *et al.* 1994) and the KRISP 94 cross-rift profile through southern Kenya from Lake Victoria towards the Chyulu Hills to the east of the rift, (Byrne *et al*. 1997) also observed a second reflector approximately 15 km deeper than the first. The reflector underlies the crust beneath the rift flanks and beneath the rift itself in both northern Ethiopia and Kenya, and in southern Kenya it underlies both Proterozoic and Archaean terranes. Beneath those rifts involving small amounts of extension, the reflection is apparently shallower by a few kilometres beneath the rift itself than beneath the rift flanks. The reflector identified beneath the northern end of Line 2 in southwestern Afar rises by about 20 km beneath the highly thinned crust at the northeastern end of this profile.

Makris & Ginzburg (1987) offer evidence that the mantle reflector continues at least 10 km north of our Line 2 (their Profile III), and less convincingly across Afar to the Danakil Horst (their Profile IV, inset to Fig. 2). While the situation beneath the along-axis profile beneath the eastern (Kenya) rift is well documented, it is not impossible for the reflector identified ~25 km beneath the thick southern section of this rift (Keller *et al.* 1994) to be correlated with the one identified at a similar depth beneath the thinned crust at the northern end of the KRISP along-axis profile rather than a deeper mantle interface.

Levin & Park (2000) provide a brief review of the possible origins of mantle discontinuities in the 50–100 km depth range:

- the phase change from spinel peridotite to garnet peridotite (Hales 1969);
- anisotropy from localized shear zones (Fuchs 1983);
- a hybrid model of localized shear developed within oceanic crust as it undergoes the gabbro-to-eclogite phase transition during shallow subduction (Bostock 1998); and
- shallow low-velocity zones (Benz & McCarthy 1994) speculatively caused by pervasive partial melt (Thybo & Perchuc 1997).

To this list we can add the interpretation of Keller *et al.* (1994) and Byrne *et al.* (1997) that the reflectors beneath the Eastern (Kenya) rift may be caused by shearing near the base of the lithosphere, separating layers resulting from subhorizontal mantle flow radiating from a region of hot mantle material rising beneath the Kenya dome in the southern Eastern (Kenya) rift.

It is not possible here to unequivocally distinguish between these hypotheses. However:

- That the mantle reflector rises up beneath extended crust, where the geotherm will be raised, is inconsistent with the pressure–temperature relationship for the spinel–garnet phase change which would result in an expected deepening of the transition as the temperature increases.
- Both the Ethiopian and the eastern (Kenya) rifts lie within the Mozambique orogenic belt, a region involved in Pan-African continental collision and possible oceanic lithospheric subduction, potentially providing conditions suitable for the hybridized model of Bostock (1998). The consistency of the reflector beneath the Ethiopian and eastern (Kenya) rifts, would suggest that there is a regional origin of the reflector rather than it resulting just from 'localized shear zones' within the sub-crustal mantle.
- Rooney *et al.* (2005) used xenoliths in Quaternary basalts in the Bishoftu and Butajira regions approximately 20 km west of the NMER to estimate the depth of melting of the host lavas at 53–88 km, equivalent to the depth of the mantle reflector discussed here. Rooney *et al.* (2005) and Furman *et al.* (2006) point out the correspondence of this depth range with the low-velocity P- and S-wave anomaly in the upper 100 km of the mantle interpreted as partial melt (Bastow *et al.* 2005). Locally, it is possible that a layer of melt may occur at the depth of the mantle reflector arising from interaction between the $P-T$ curve and solidus for the particular mantle composition. However, the reflector is at approximately the same depth beneath both the southeastern and northwestern flanks of the NMER (the former lacking, the latter having, the HVLC layer) and also within both Archaean and Proterozoic lithosphere beneath the flanks of the Eastern (Kenya) rift, with probably different $P-T$ conditions that should not allow melting at a constant depth.
- Analysis of SKS recordings and surface-wave dispersion over the NMER are not consistent with the hypothesis of the reflectors resulting from horizontal mantle flow at the top of a spreading mantle plume head (Gashawbeza *et al.* 2004). Seismic anisotropy may correlate with pre-existing Pan-African lithospheric alignment away from the rift trend (Gashawbeza *et al.* 2004; Kendall *et al.* 2006). Within the uppermost 75 km beneath the rift, the observed anisotropy is primarily due to melt alignment orientated in a rift-parallel direction (Kendall *et al.* 2005).

Hence, we believe the most likely cause of the mantle reflector is a compositional or structural boundary within pre-existing lithosphere, owing to the correlation of reflector depth with the amount of lithospheric extension, rather than a phase change or melt front.

## Conclusions

The EAGLE controlled-source project provides an intriguing new image of crustal and uppermost mantle structure beneath a 400 × 400 km region centred on the Boset magmatic segment of the transitional northern Main Ethiopian Rift (see Fig. 8).

The sedimentary–volcanic layer delineated on the along-axis and cross-rift profiles shows that the Mesozoic sedimentary rocks and Tertiary to Recent volcanics in both the rift and the flanking plateaus have a combined maximum thickness of >5 km. Basement topography shows that the bounding faults extend into the crystalline basement, as identified for example on the southeastern

flank of the Adama basin. Along the axis of the rift, the total thickness of the sediment–volcanic layer is fairly constant at about 5 km, but its two units vary in thickness considerably. This may be a result of the location of the seismic line and its passage through along-axis sub-basins, or may truly reflect simple basement architecture in this transitional rift.

The upper crust exhibits normal continental crustal velocities ($V_p$ *c*. 6.1 km s$^{-1}$) except beneath the magmatic segments within the rift, where higher-than-normal upper-crustal velocities are interpreted to result from mafic intrusions beneath the magmatic centres. The magmatic segmentation is identified to mid-crustal levels and possibly into the lower crust. While there is a possible correlation between anomalous low-velocity mantle segmentation and rift valley structural segmentation, the process by which melt transport is transferred from the mantle to a crustal region dominated by magmatic segmentation is not yet resolved.

A 40 km-thick crust with normal continental velocity structure lies above normal upper mantle ($V_p$ 8.05 km s$^{-1}$) on the plateau southeast of the rift valley. Beneath the plateau NW of the rift, a 48 km-thick crystalline crust includes a 15 km-thick high-velocity ($V_p$ 7.4 km s$^{-1}$) layer that is interpreted as underplate associated with the Oligocene flood basalt and more recent magmatic activity. Along the axis of the rift, the sub-Moho velocities are *c*. 7.5 km s$^{-1}$ interpreted as resulting from raised mantle temperatures and a small percentage of partial melt. The crust thins significantly over a 50 km distance from *c*. 40 km in the SW to 26 km at the NE end of the EAGLE axial seismic profile, and the thinning primarily occurs in the upper crust. The apparently uniform velocity of the lower crust may mask an increase in mafic intrusions in the highly extended crust beneath Afar as a result of a higher geotherm. Our model of the crust along the axis of the NMER can in fact be explained from SW to NE in terms of rifted continental crust transitioning into thick, possibly near total igneous crust above a high-temperature mantle providing the necessary basaltic melt. The results from this and other EAGLE studies strongly support the magma-assisted rifting hypothesis of Buck (2004).

A mantle reflector has been identified at a depth of about 60 km beneath the plateaus that bound the rift valley. A correlative reflector is apparently slightly shallower beneath the southern part of the rift and at *c*. 40 km beneath the highly extended northeastern end of the axial profile in southern Afar. While it is not possible to be definitive as to its cause, because its depth apparently correlates with the amount of extension, we believe that it most likely represents a compositional or structural boundary. The fact that an equivalent reflector has been observed beneath the eastern (Kenya) rift and further north in Afar strongly suggests that this may be an important observation with generic implications for the origin and development of magmatic continental rifts and subsequent volcanic margins.

We would like to acknowledge the support, work and many discussions held variously with C. Ebinger, G. Stuart, J.M. Kendall, M. Fowler, A. Ayele, I. Bastow, A. Brisbourne, D. Cornwell, P. Denton, E. Gashaw-Beza, D. Keir, K. Mickus, T. Mammo & K. Tadesse. In addition to these and the authors, participants in the EAGLE project came from:

*Ethiopia*: Addis Ababa University, Ethiopian Geological Survey, Ethiopian Petroleum Operations Department, Ethiopian Commission for Science and Technology, Oromia Council, Addis Ababa.

*Europe*: University of Leicester, University of London, Royal Holloway, University of Leeds, SEIS-UK, University of Edinburgh, University of Copenhagen, Dublin Institute for Advanced Studies, University of Vienna, University of Stuttgart.

*USA*: Stanford University, University of Texas at El Paso, Pennsylvania State University, Missouri State University, US Geological Survey, University of Colorado at Boulder.

Figures 1, 2, 3, 4, 5 & 7 involved the use GMT software (Wessel & Smith 1995). Helpful reviews were provided by C. Ebinger, D. Lizarralde and W. Mooney. Funding for the EAGLE project was provided by NERC (NER/A/S/2000/00563,01003,01004), the National Science Foundation Continental Dynamics program EAR 0208475, the Texas Higher Education Coordinating Board, the Royal Society and the University of Leicester. Instrumentation was provided by SEIS-UK, IRIS-PASSCAL and the University of Copenhagen.

## References

ABDELSALAM, M.G. & STERN, R.J. 1996. Sutures and shear zones in the Arabian–Nubian shield. *Journal of African Earth Sciences*, **23**, 289–310.

ALLEN, A. & TADESSE, G. 2003. Geological setting and tectonic subdivision of the Neoproterozoic orogenic belt of Tuludimtu, western Ethiopia. *Journal of African Earth Sciences*, **36**, 329–343.

AYALEW, D., BARBEY, P., MARTY, B., REISBERG, L., YIRGU, G. & PIK, R. 2002. Source, genesis and timing of giant ignimbrite deposits associated with Ethiopian continental flood basalts. *Geochimica et Cosmochimica Acta*, **66**, 1429–1448.

AYALEW, D., EBINGER, C., BOURDON, E., WOLFENDEN, E., YIRGU, G. & GRASSINEAU, N. 2006. Temporal compositional variation of syn-rift rhyolites along the southwestern margin of the Red Sea and northern Main Ethiopian Rift. *In*: YIRGU, G.,

EBINGER, C.J. & MAGUIRE, P.K.H. (eds) *The Afar Volcanic Province within the East African Rift System.* Geological Society, London, Special Publications, **259**, 121–130.

AYELE, A., STUART, G. & KENDALL, J.-M. 2004. Insights into rifting from shear wave splitting and receiver functions; an example from Ethiopia. *Geophysical Journal International*, **157**, 354–362.

BASTOW, I.D., STUART, G.W., KENDALL, J.-M. & EBINGER, C.J. 2005. Upper mantle seismic structure in a region of incipient continental break-up: northern Ethiopian rift. *Geophysical Journal International*, **162**, 479–493 doi:10.1111/j.1365-246x.2005.02666.x.

BENDICK, R., MCCLUSKY, S., BILHAM, R., ASFAW, L. & KLEMPERER, S.L. 2006. Distributed Nubia–Somalia relative motion and dike intrusion in the Main Ethiopian Rift. *Geophysical Journal International* (in press).

BENOIT, M.H., NYBLADE, A.A. & VANDECAR, J.C. 2006. Upper mantle P wave speed variations beneath Ethiopia and the origin of the Afar Hotspot. *Geology* (in press).

BENZ, H.M. & MCCARTHY, J. 1994. Evidence for an upper mantle low velocity zone beneath the southern Basin and Range–Colorado plateau transition zone. *Geophysical Research Letters*, **21**, 509–512.

BERCKHEMER, H., BAIER, B., *ET AL.* 1975. Deep seismic soundings in the Afar region and on the highland of Ethiopia. *In*: PILGER, A. & RÖSLER, A. (eds) *Afar Depression of Ethiopia*. Schweizerbart, Stuttgart, **I**, 89–107.

BILHAM, R., BENDICK, R., LARSON, K., MOHR, P., BRAUN, J., TESFAYE, S. & ASFAW, L. 1999. Secular and tidal strain across the Main Ethiopian Rift. *Geophysical Research Letters*, **26**, 2789–2792.

BIRT, C.S., MAGUIRE, P.K.H., KHAN, M.A., THYBO, H., KELLER, G.R. & PATEL, J. 1997. The influence of pre-existing structures on the evolution of the southern Kenya Rift Valley—evidence from seismic and gravity studies. *Tectonophysics*, **278**, 211–242.

BOCCALETTI, M., MAZZUOLI, R., BONINI, M., TRUA, T. & ABEBE, B. 1999. Plio-Quaternary volcanotectonic activity in the northern sector of the Main Ethiopian Rift: relationships with oblique rifting. *Journal of African Earth Sciences*, **29**, 679–698.

BONINI, M., CORTI, G. INNOCENTI, F., MANETTI, P., MAZZARINI, F., TSEGAYE ABEBE, T. & PECSKAY, Z. 2005. Evolution of the Main Ethiopian Rift in the frame of Afar and Kenya rifts propagation. *Tectonics*, **24**, TC1007, 10.1029/2004TC001680,

BOSELLINI, A., RUSSO, A. & ASSEFA, G. 2001. The Mesozoic succession of Dire Dawa, Harar Province, Ethiopia. *Journal of African Earth Sciences*, **32**, 403–417.

BOSTOCK, M.G. 1998. Mantle stratigraphy and the evolution of the Slave province. *Journal of Geophysical Research*, **103**, 21183–21200.

BROCHER, T.M. 2005. Empirical relations between elastic wavespeeds and density in the Earth's crust. *Bulletin of the Seismological Society of America*, **95**, 2081–2092.

BUCK, W.R. 2004. Consequences of asthenospheric variability on continental rifting. *In*: KARNER, G.D., TAYLOR, B., DRISCOLL, N.W. & KOHLSTEDT, D.L. (eds) *Rheology and Deformation of the Lithosphere at Continental Margins*, Columbia University Press, New York, pp. 1–30.

BYRNE, G.F., JACOB, A.W.B., MECHIE, J. & DINDI, E. 1997. Seismic structure of the upper mantle beneath the southern Kenya Rift from wide-angle data. *Tectonophysics*, **278**, 243–260.

CHERNET, T., HART, W., ARONSON, J. & WALTER, R. 1998. New age constraints on the timing of volcanism and tectonism in the northern Main Ethiopian Rift – southern Afar transition zone (Ethiopia). *Journal of Volcanology and Geothermal Research*, **80**, 267–280.

CORNWELL, D.G., MACKENZIE, G.D., MAGUIRE, P.K.H., ENGLAND, R.W., ASFAW, L. & OLUMA, B. 2006. Northern Main Ethiopian Rift crustal structure from new high-precision gravity data. *In*: YIRGU, G., EBINGER, C.J. & MAGUIRE, P.K.H. (eds) *The Afar Volcanic Province within the East African Rift System*. Geological Society, London, Special Publications, **259**, 307–321.

D'ACREMONT, E., LEROY, S., BESLIER, M.-O., BELLAHSEN, N., FOURNIER, M., ROBIN, C., MAIA, M. & GENTE, P. 2005. Structure and evolution of the eastern Gulf of Aden conjugate margins from seismic reflection data. *Geophysical Journal International*, **160**, 869–890, doi: 10.1111/j.1365-246X.2005.02524.x.

DEEMER, S.J. & HURICH, C.A. 1994. The reflectivity of magmatic underplating using the layered mafic intrusion analog. *Tectonophysics*, **232**, 239–255.

DUGDA, M., NYBLADE, A., JULIA, J., LANGSTON, C., AMMON, C. & SIMIYU, S. 2005. Crustal structure in Ethiopia and Kenya from receiver function analysis: implications for rift development in eastern Africa. *Journal of Geophysical Research*, **110**, B101303, doi:10.1029/2004JB003065.

EAGLES, G., GLOAGUEN, R. & EBINGER, C.J. 2002. Kinematics of the Danakil microplate. *Earth and Planetary Science Letters*, **203**, 607–620.

EBINGER, C.J. & CASEY, M. 2001. Continental breakup in magmatic provinces: An Ethiopian example. *Geology*, **29**, 527–530.

FUCHS, K. 1983. Recently formed elastic anisotropy and petrological models for the continental subcrustal lithosphere in southern Germany. *Physics of the Earth and Planetary Interiors*, **31**, 93–118.

FURMAN, T., BRYCE, J., ROONEY, T., HANAN, B., YIRGU, G. & AYALEW, D. 2006. Heads and tails: 30 million years of the Afar plume. *In*: YIRGU, G., EBINGER, C.J. & MAGUIRE, P.K.H. (eds) *The Afar Volcanic Province within the East African Rift System.* Geological Society, London, Special Publications, **259**, 95–119.

GAO, W., GRAND, S., BALDRIDGE, W., WILSON, D., WEST, M., NI, J. & ASTER, R. 2004. Upper mantle convection beneath the central Rio Grande rift imaged by P and S wave tomography. *Journal*

*of Geophysical Research*, **109**, B03305, doi: 10.1029/2003 JB002743.

GASHAWBEZA, E.M., KLEMPERER, S.L., NYBLADE, A.A., WALKER, K.T. & KERANEN, K.M. 2004. Shear-wave splitting in Ethiopia: Precambrian mantle anisotropy locally modified by Neogene rifting. *Geophysical Research Letters*, **31**, L18602, doi:10.1029/2004GL020471.

HALES, A.L. 1969. A seismic discontinuity in the lithosphere. *Earth and Planetary Science Letters*, **7**, 44–46.

HEBERT, L. & LANGSTON, C. 1984. Crustal thickness estimate at AAE (Addis Ababa, Ethiopia) and NAI (Nairobi, Kenya) using teleseismic P-wave conversions. *Tectonophysics*, **111**, 299–327.

HOLE, J.A. 1992. Nonlinear high-resolution three-dimensional seismic travel time tomography. *Journal of Geophysical Research*, **97**, 6553–6562.

HORNER-JOHNSTON, B.C., GORDON, R.G., COWLES, S.M. & ARGUS, D.F. 2003. The angular velocity of Nubia relative to Somalia and the location of the Nubia–Somalia–Antarctica triple junction. *EOS Transactions American Geophysical Union*, **84**(6), abs T52F-01.

KEIR, D., KENDALL, J.-M., EBINGER, C. & STUART, G. 2005. Variations in late syn-rift melt alignment inferred from shear-wave splitting in crustal earthquakes beneath the Ethiopian rift. *Geophysical Research Letters* **32**, L23308, doi: 10.1029/2005GL024150.

KEIR, D., EBINGER, C., STUART, G., DALY, E. & AYELE, A. 2006. Strain accommodation by magmatism and faulting as rifting proceeds to breakup: Seismicity of the northern Ethiopian Rift. *Journal of Geophysical Research* (in press).

KELEMEN, P.B. & HOLBROOK, W.S. 1995. Origin of thick high-velocity igneous crust along the U.S. East coast margin. *Journal of Geophysical Research*, **100**, 10077–10094.

KELLER, G.R., MECHIE, J., BRAILE, L., MOONEY, W.D. & PRODEHL, C. 1994. Seismic structure of the uppermost mantle beneath the Kenya Rift. *Tectonophysics*, **236**, 201–216.

KENDALL, J.-M., PILIDOU, S., KEIR, D., BASTOW, I.D., STUART, G.W. & AYELE, A. 2006. Mantle upwellings, melt migration and the rifting of Africa: Insights from seismic anisotropy. *In*: YIRGU, G., EBINGER, C.J. & MAGUIRE, P.K.H. (eds) *The Afar Volcanic Province within the East African Rift System.* Geological Society, London, Special Publications, **259**, 55–72.

KENDALL, J.-M., STUART, G., EBINGER, C., BASTOW, I. & KEIR, D. 2005. Magma-assisted rifting in Ethiopia. *Nature*, **433**, 146–148.

KERANEN, K., KLEMPERER, S.L., GLOAGUEN, R. & the EAGLE Working Group. 2004. Imaging a proto-ridge axis in the Main Ethiopian Rift. *Geology*, **32**, 949–952.

KORME, T., ACOCELLA, V. & ABEBE, B. 2004. The role of pre-existing structures in the origin, propagation and architecture of the faults in the Main Ethiopian Rift. *Gondwana Research*, **7**, 467–479.

LEVIN, V. & PARK, J. 2000. Shear zones in the Proterozoic lithosphere of the Arabian shield and the nature of the Hales discontinuity. *Tectonophysics*, **232**, 131–148.

MACKENZIE, G.D., THYBO, H. & MAGUIRE, P.K.H. 2005. Crustal velocity structure across the Main Ethiopian Rift: Results from 2-dimensional wide-angle seismic modelling. *Geophysical Journal International*, **162**, 994–1006 doi: 10.1111/j.1365-246X.2005. 02710.x.

MAGUIRE, P.K.H., SWAIN, C.J., MASOTTI, R. & KHAN, M.A. 1994. A crustal and uppermost mantle cross-sectional model of the Kenya Rift derived from seismic and gravity-data. *Tectonophysics*, **236**, 217–249.

MAGUIRE, P., EBINGER, C., *ET AL.* 2003. Geophysics project in Ethiopia studies continental breakup. *EOS Transactions American Geophysical Union*, **84**, 342–343.

MAHATSENTE, R., JENTZSCH, G. & JAHR, T. 1999. Crustal structure of the Main Ethiopian Rift from gravity data: 3-dimensional modelling. *Tectonophysics*, **313**, 363–382.

MAKRIS, J. & GINZBURG, A. 1987. The Afar Depression: transition between continental rifting and sea floor spreading, *Tectonophysics*, **141**, 199–214.

MECHIE, J., KELLER, G.R., PRODEHL, C., GACIRI, S., BRAILE, L.W., MOONEY, W.D., GAJEWSKI, D. & SANDMEIER, K.-J. 1994*a*. Crustal structure beneath the Kenya Rift from axial profile data. *Tectonophysics*, **236**, 179–200.

MECHIE, J., FUCHS, K. & ALTHERR, R. 1994*b*. The relationship between seismic velocity, mineral composition and temperature and pressure in the upper-mantle – with an application to the Kenya Rift and its eastern flank. *Tectonophysics*, **236**, 453–464.

MENZIES, M.A., KLEMPERER, S.L., EBINGER, C.J. & BAKER, J. 2002. Characteristics of volcanic rifted margins. *In*: MENZIES, M.A., KLEMPERER, S.L., EBINGER, C. & BAKER, J. (eds) *Magmatic Rifted Margins.* Geological Society of America Special Paper, **362**, pp. 1–14.

MOHR, P.A. & ZANETTIN, B. 1988. The Ethiopian flood basalt province. *In*: (ANON.) *Continental Flood Basalts*. Kluwer Academy, Dordrecht, Netherlands, 63–110.

MONTELLI, R., NOLET, G., DAHLEN, F.A., MASTERS, G., ENGDAHL, E.R. & HUNG, S.-H. 2004. Finite frequency tomography reveals a variety of plumes in the mantle. *Science*, **303**, 338–343.

NYBLADE, A.A. 2002. Crust and upper mantle structure in East Africa; implications for the origin of Cenozoic rifting and volcanism and the formation of magmatic rifted margins. *In*: MENZIES, M.A., KLEMPERER, S.L., EBINGER, C.J. & BAKER, J. (eds) *Volcanic Rifted Margins.* Geological Society of America, Special Paper, **362**, 15–26.

NYBLADE, A.A. & SLEEP, N.H. 2003. Long lasting epeirogenic uplift from mantle plumes and the origin of the Southern African Plateau. *Geochemistry, Geophysics, Geosystems*, **4**, 1105, doi:10.1029/2003GC000573.

PIK, R., MARTY, B., CARIGNAN, J. & LAVÉ, J. 2003. Stability of the Upper Nile drainage network

(Ethiopia) deduced from (U–Th)/He thermochronometry: implications for uplift and erosion of the Afar plume dome. *Earth and Planetary Science Letters*, **215**, 73–88.

PRODEHL, C., JACOB, A.W.B., THYBO, H., DINDI, E. & STANGL, R. 1994. Crustal structure on the northeastern flank of the Kenya rift. *Tectonophysics*, **236**, 271–290.

PRODEHL, C., FUCHS, K. & MECHIE, J. 1997. Seismic-refraction studies of the Afro-Arabian rift system – a brief review. *Tectonophysics*, **278**, 1–13.

ROONEY, T.O., FURMAN, T., YIRGU, G. & AYELEW, D. 2005. Structure of the Ethiopian lithosphere: Evidence from mantle xenoliths. *Geochimica et Cosmochimica Acta*, **69**(15), 3889–3910. doi:10.1016/j/gca.2005.03.043.

SCHULL, T.J. 1988. Rift basins of interior Sudan; petroleum exploration and discovery. *American Association for Petroleum Geologists Bulletin*, **72**, 1128–1142.

STERN, R.J. 1994. Arc assembly and continental collision in the Neoproterozoic East African orogeny implications for the consolidation of Gondwana. *Annual Review of Earth and Planetary Sciences*, **22**, 319–351.

STUART, G.W., BASTOW, I.D. & EBINGER, C.J. 2006. Crustal structure of the northern Ethiopian Rift from receiver function studies. *In*: YIRGU, G., EBINGER, C.J. & MAGUIRE, P.K.H. (eds) *The Afar Volcanic Province within the East African Rift System.* Geological Society, London, Special Publications, **259**, 253–267.

TADESSE, S., MILESI, J.-P. & DESCHAMPS, Y. 2003. Geology and mineral potential of Ethiopia: a note on the geology and mineral map of Ethiopia. *Journal African Earth Sciences*, **36**, 273–313.

TIBERI, C., EBINGER, C., BALLU, V., STUART, G. & OLUMA, B. 2005. Inverse models of gravity data from the Red Sea–Aden–East African rifts triple junction zone. *Geophysical Journal International*, **63**, 775–787.

THYBO, H. & PERCHUC, E. 1997. The seismic 8° discontinuity and partial melting in continental mantle. *Science*, **257**, 1626–1629.

THYBO, H., MAGUIRE, P.K.H., BIRT, C.S. & PERCHUC, E. 2000. Seismic reflectivity and magmatic underplating beneath the Kenya Rift. *Geophysical Research Letters*, **27**, 2745–2749.

TRUA, T., DENIEL, C. & MAZZUOLI, R. 1999. Crustal control in the genesis of Plio-Quaternary bimodal magmatism of the Main Ethiopian Rift (MER): geochemical and isotopic (Sr, Nd, Pb) evidence. *Chemical Geology*, **155**, 201–231.

WESSEL, P. & SMITH, W.H.F. 1995. New version of the Generic Mapping Tools released. *EOS Transactions American Geophysical Union*, **76**, 329.

WHALER, K.A. & HAUTOT, S. 2006. The electrical resistivity structure of the crust beneath the northern Main Ethiopian Rift (EAGLE Phase III). *In*: YIRGU, G., EBINGER, C.J. & MAGUIRE, P.K.H. (eds) *The Afar Volcanic Province within the East African Rift System.* Geological Society, London, Special Publications, **259**, 293–305.

WHITE, R.S. & MCKENZIE, D. 1995. Mantle plumes and flood basalts. *Journal of Geophysical Research*, **100**, 17543–17585.

WOLFENDEN, E., EBINGER, C., YIRGU, G., DEINO, A. & AYALEW, D. 2004. Evolution of the northern Main Ethiopian Rift: birth of a triple junction. *Earth and Planetary Science Letters*, **224**, 213–228.

ZELT, C.A. & FORSYTH, D.A. 1994. Modeling of wide-angle seismic data for crustal structure: Southeastern Grenville Province. *Journal of Geophysical Research*, **99**, 11687–11704.

ZELT, C.A. & SMITH, R.B. 1992. Seismic traveltime inversion for 2-D crustal velocity structure. *Geophysical Journal International*, **108**, 16–34.